Whole Brain 3D Spectroscopic Mapping of Isocitrate Dehydrogenase Mutant Glioma.

Aysha Alsahlawi

Department of Human Genetics, Faculty of Medicine and Health Sciences, McGill University, Montreal, Quebec, Canada

June 2023

A thesis submitted to the McGill University in partial fulfillment of the requirements of the

degree of Master of Science.

© Aysha Alsahlawi, 202

Table of Contents

Abstract

Isocitrate dehydrogenase (IDH) enzymes are a key element in the Krebs cycle and therefore cellular homoeostasis. Whole brain three-dimensional spectroscopic imaging is a feasible tool to display global metabolic reprogramming driven by IDH mutation seen in gliomas. We conducted a prospective longitudinal observational study recruiting WHO grade II-IV IDH mutant and IDH wildtype glioma patients undergoing surgical resection at the Montreal Neurological Institute. MIDAS software was used for processing and segmentation of three-dimensional echoplanar spectroscopic imaging obtained pre-operatively and 2 weeks after surgery. Parametric maps of N-Acetylspartate (NAA), Choline, GLX (Glutamine +Glutamate), Creatine and lactate were computed and co-registered on FLAIR images using MRIcrogl software. In total, 8 patients were recruited (5 IDH mutant and 3 IDH Wildtype) as well as 4 healthy controls. We analyzed the mean regional concentrations (Choline, Creatine, Lactate, NAA, GLX, Glu, Gln) and LAC/NAA, Cho/NAA ratios for 26 regions of interest (ROI) including tumoral, peritumoral and contralateral areas. Compared to healthy control and IDH wildtype, IDH mutant tumoral area showed a drop in the concentration of glutamate (P=0.025) with higher levels of glutamine (P=0.001), Choline (P=0.001) and overall reduction in GLX concentration (P=0.018). IDH wild-type tumoral area showed higher concentration of lactate (P=0.001). Among IDH mutants, peritumoral area had significant drop of choline (P=0.001) and Taurine (0.027), higher concentration of glutamate (P=0.001) with lower Cho/NAA ratios below 1. Post-operatively, Glutamate was higher at the surgical margin when compared to pre-operative peritumoral areas (0.023). Analysis of contralateral areas showed no significant difference in the metabolites of interest for both IDH mutant and wildtype glioma. Taken all together, these metabolic changes reflect an IDH-mediated increase in cellular density with higher energy demand captured in these

tumors. Additionally, metabolic changes seen in peritumoral area could offer a potential marker for tumor border guiding surgical resection. Furthermore, whole brain spectroscopy offers a potential tool in IDH mutant post-operative assessment. Finally, in the absence of contralateral metabolic alterations, we suggest that IDH mutation affect tumoral and peritumoral area metabolites with no global impact detected.

Résumé

Les enzymes isocitrate déshydrogénase (IDH) sont un élément clé du cycle de Krebs et donc de l'homéostasie cellulaire. L'imagerie spectroscopique tridimensionnelle de l'ensemble du cerveau est un outil viable pour afficher la reprogrammation métabolique globale induite par la mutation IDH observée dans les gliomes. Nous avons mené une étude observationnelle longitudinale prospective recrutant des patients atteints de gliome IDH mutant de grade II-IV de l'OMS et de type sauvage IDH subissant une résection chirurgicale à l'Institut Neurologique de Montréal. Le logiciel MIDAS a été utilisé pour le traitement et la segmentation de l'imagerie spectroscopique échoplanar tridimensionnelle obtenue avant l'opération et 2 semaines après la chirurgie. Les cartes paramétriques de N-Acétylspartate (NAA), Choline, GLX (Glutamine + Glutamate), Créatine et lactate ont été calculées et co-enregistrées sur les images FLAIR en utilisant le logiciel MRIcrogl. Au total, 8 patients ont été recrutés (5 mutants IDH et 3 de type sauvage IDH) ainsi que 4 individus en bonne santé. Nous avons analysé les concentrations régionales moyennes (Choline, Créatine, Lactate, NAA, GLX, Glu, Gln) et les rapports LAC/NAA, Cho/NAA pour 26 régions d'intérêt (ROI) comprenant des zones tumorales, péritumorales et controlatérales. Comparée au contrôle sain et au type sauvage IDH, la zone tumorale mutant IDH a montré une baisse de la concentration de glutamate (P=0,025) avec des niveaux plus élevés de glutamine (P=0,001), de choline (P=0,001) et une réduction globale de la concentration de GLX (P=0,018). La zone tumorale de type sauvage IDH a montré une concentration plus élevée de lactate (P=0,001). Parmi les mutants IDH, la zone péritumorale a connu une baisse significative de choline (P=0,001) et de Taurine (0,027), une concentration plus élevée de glutamate (P=0,001) avec des ratios Cho/NAA inférieurs à 1. Post-opératoirement, le Glutamate était plus élevé à la marge chirurgicale par rapport aux zones péritumorales préopératoires (0,023).

L'analyse des zones controlatérales n'a montré aucune différence significative dans les métabolites d'intérêt pour le gliome mutant IDH et de type sauvage. Globalement, ces changements métaboliques reflètent une augmentation de la densité cellulaire médiée par IDH avec une demande énergétique plus élevée capturée dans ces tumeurs. De plus, les changements métaboliques observés dans la zone péritumorale pourraient offrir un marqueur potentiel pour la bordure tumorale guidant la résection chirurgicale. De plus, la spectroscopie du cerveau entier offre un outil potentiel dans l'évaluation postopératoire des mutants IDH. Enfin, en l'absence d'altérations métaboliques controlatérales, nous suggérons que la mutation IDH affecte les métabolites de la zone tumorale et péritumorale sans impact global détecté.

Acknowledgments

As I reflect on the journey, I have undertaken to complete this thesis, it is with profound gratitude that I acknowledge the invaluable guidance and support of my supervisors, Dr. Roberto Diaz and Dr. Nada Jabado. The unique combination of their areas of expertise has provided a synergistic platform for the execution of translational research. Through their mentorship, I have gained a rich understanding of the interplay between science and neurosurgical clinical practice, and the vital role it plays in advancing patient care.

I extend my sincere gratitude to Drs. Livia Garzia and Sridar Narayanan, who serve on the committee. their insightful criticism, incisive suggestions, and profound wisdom have immeasurably enriched this work. their knowledge, expertise, and attention to detail were instrumental in shaping the final form of this thesis.

Special thanks go to my Neurosurgery Programme Director, Jeffrey Atkinson, whose unwavering support and understanding have been instrumental in allowing me to pursue this master's degree concurrently with my neurosurgical residency training, thereby fostering an environment that encourages both clinical and academic growth.

Lastly, I wish to dedicate this thesis to all those who bravely battle glioma. It is my hope that this research will contribute to a more in-depth understanding of the disease and improve surgical outcome for our patients.

Contribution of authors

MIDAS (Metabolic Imaging Data Analysis System) software Processing files and parameters MRS acquisition were written in collaboration with Dr. Jamie Near and Mr. Brenden Kadota from The Douglas Research Centre at McGill University. Navigating MIDAS software was feasible by consulting the software developers Dr. Maudsley, Andrew and Dr. Sheriff, Sulaiman Ahmed from Miller School of Medicine University of Miami. Patients recruitment, data interpretation, analysis, spectrum fitting, heatmaps generation, segmentation and writing the thesis have been done by me.

List of figures

List of tables

List of Abbreviations

Isocitrate dehydrogenases (IDH)

Three-dimensional echoplanar spectroscopic imaging (3D EPSI)

alpha-ketoglutarate (α-KG)

Nicotinamide adenine dinucleotide phosphate (NADP+)

2-Hydroxyglutarate (2HG).

Tricarboxylic acid (TCA)

Jumonji C (JmjC)

Ten-eleven translocation enzymes (TETs)

N-Acetyl aspartic acid (NAA)

Choline-containing compounds (tCho)

Free choline (Cho)

Glycerophoshorylcholine (GPC)

Phosphorylcholine (PC)

Lactate (Lac)

Glutamate (Glu)

Glutamine (Gln)

γ-Aminobutyric acid (GABA)

Taurine (Tau)

Creatine (Cr)

Mitochondrial creatine kinase (MtCK),

Single-voxel spectroscopy (SVS)

3-Dimensional magnetic resonance imaging (3D-MRI)

Tumor-associated macrophages (TAMs)

Glioblastoma-associated stromal cells (GASCs)

Lactate-to-N-acetyl-aspartate ratio (Lac/NAA)

Choline/N-acetyl-aspartate ratio (Cho/NAA)

Glutamate and glutamine (Glx)

Karnofsky Performance Scale (KPS)

Magnetic Resonance Spectroscopy Imaging (MRSI)

Fluid attenuated inversion recovery (FLAIR)

MIDAS (Metabolic Imaging Data Analysis System)

Four-Dimensional Fourier Transform (FDFT)

Automated spectral fitting of single spectra (FITT)

Reference MRSI Data Formation (REFDAT)

Regions of interest (ROI)

Tumoral (tROI)

Peritumoral area (pROI)

Contralateral brain (cROI)

Post-operative (post-opROI)

Raw Digital Imaging and Communications in Medicine (DICOM)

Low Grade Glioma (LGG)

High Grade Glioma (HGG)

N-*acetyl*-aspartyl-glutamate (NAAG)

Chapter 1: Introduction

It has become evident that gliomas transcend the boundary delineated by the T2 signal change.(1-3) Understanding the metabolic reprogramming driven by the tumor beyond its radiological margin will provide further insights into the tumorigenesis of gliomas. The primary objective of our study is to capture the global metabolic changes in brain metabolites for both Isocitrate dehydrogenases (IDH) mutant and wild type gliomas.

One emerging modality is three-dimensional echoplanar spectroscopic imaging (3D EPSI)(4, 5). In this study, we employed this recent technology to analyze various metabolites detected in tumoral, peritumoral and contralateral areas for IDH mutant and IDH wild-type tumors before and after surgical resection. By studying these metabolites and their spatial distribution, we aim to shed light on the multifaceted metabolic complexities of gliomas, and ultimately contribute to a more targeted resection of these tumors.

1.1 Isocitrate dehydrogenases mutation

Since reported in 2008-2009 (6), isocitrate dehydrogenases mutation types IDH1/2 which are present in up to 70–80% of infiltrating gliomas have fundamentally changed the way adult-type gliomas are being classified given their impact on epigenetics, tumor microenvironment and patients survival (7, 8). Thus, the updated 2021WHO classification was based on the notion that IDH-mutant delivers a less heterogeneous approach in predicting prognosis and treatment response than histological factors such as the degree of necrosis or microvascular proliferation (9). Based on 2021WHO classification, tumors categorized into Astrocytoma - IDH-mutant, Oligodendroglioma - IDH-mutant, 1p/19q-codeleted, and Glioblastoma. In recently published data from the United States National Cancer Database, one-year overall-survival (OS) was 53.7% for WHO grade 4 IDH-wildtype glioblastomas; 98.0%, 92.4%, and 76.3% for WHO

grade 2, 3, and 4 IDH-mutant astrocytomas, respectively; 97.9% and 94.4% for WHO grade 2 and 3 IDH-mutant 1p/19q-codeleted oligodendrogliomas, respectively (10).

Located on 2q33 and 15q26, both isocitrate dehydrogenase 1 (IDH1- cytoplasm) and isocitrate dehydrogenase 2 (IDH2- mitochondria) function as single-gene enzymes in citric acid cycle, by oxidizing isocitrate to alpha-ketoglutarate (α-KG) which leads to the generation NADPH through utilizing nicotinamide adenine dinucleotide phosphate (NADP+) (6, 11). In the case of IDH mutation, a substitution at one of two active enzymatic sites, typically from arginine to histidine develops a gain-of-function ability to convert α-ketoglutarate into 2-hydroxyglutarate (2HG) while the wild-type form continues to produce α-ketoglutarate (12). In this study, we aim to capture metabolic changes associated with IDH mutant glioma as a result of cellular metabolism forced to compensate for the shortage in α-ketoglutarate and NADPH (13) (11).

1.2 2-hydroxyglutarate

As a result of IDH1/2 mutations, oncometabolite 2-hydroxyglutarate (2HG) accumulates within the tumor cells (14). Dang *et al* demonstrated that mutant IDH1 tumors had between 5 and 35 μmol of 2HG per gram of tumor, in contrast IDH wild-type tumor IDH1 had over 100-fold less 2HG (12). The downstream effect of 2HG accumulation remains an area of interest. One hypothesis is that 2HG competitively inhibit α-ketoglutarate–dependent enzymes resulting in tricarboxylic acid (TCA) cycle down-regulation which leads to deregulating of ATP synthase (15). 2-hydroxyglutarate competitively inhibits numerous α-KG-dependent-dixoxygenases and also Jumonji C (JmjC) domain-containing histone demethylase (JHDM)s and ten-eleven translocation enzymes (TETs 1/2), which leads to histone and DNA methylation. 2-HG also

inhibits ALKBHs, which disrupt DNA repair of methylation damage (16). These findings raise the question as to how 2-HG would impact global metabolism in IDH mutant gliomas compared to IDH wild-type.

1.3 Cellular metabolism

In the realm of glioma research, widespread metabolic disturbances of the cellular metabolism have been identified(17, 18). This includes disturbances in key metabolites such as choline, glutamine/glutamate, and N-acetylated amino acids (19, 20). However, the intricate dynamics and full implications of these metabolic disruptions in relation to IDH mutation remain an area for further exploration

1.3.1 N-Acetylated Amino Acids

One of the most concentrated metabolites found in the brain is N-acetyl aspartic acid (NAA) (21). Synthesized from aspartate and acetyl-coenzyme A, NAA found only in neurons is a key element in the nervous system metabolism. In a healthy brain, NAA concentration varies between 6–11 mM (22). The exact role of NAA is still unclear but it has been reported to be involved in osmoregulation, myelin lipid synthesis and axon-glial signaling (23). Interestingly, NAA has also been linked to ATP metabolism and energy production by favoring the conversion of glutamate to alpha ketoglutarate through acetylation of aspartate (24). Reduced levels of NAA reported in cases of stroke, tumors, and multiple sclerosis support the notion that NAA is a marker of neuronal integrity and can be used as a surrogate for neuronal loss and dysfunction (25).

1.3.2 Choline

Choline-containing compounds (tCho) including free choline (Cho), glycerophoshorylcholine (GPC), and phosphorylcholine (PC), are involved phospholipid synthesis and degradation pathways (26). Consequently, Choline has been used to reflect membrane turnover as a marker of cellular density. The concentration of tCho in human brain is approximately 1–2 mM.(27, 28)

1.3.3 Lactate

In a healthy brain, lactate is present at a very low concentration of 0.5 mM (29). As a critical step in glycolysis, lactate dehydrogenase (LDH) converts pyruvate to lactate. An environment with rapidly proliferating cells relies heavily on glycolysis, a concept referred to as the "Warburg effect(30)". In response to this hypoxic microenvironment, increase expression level of LDH has been reported which furthermore promote cell proliferation, migration and invasion (31). In adaptation to hypoxia, cells mediate the expression of multiple transcription factors most importantly hypoxia-inducible factor (HIF)-1α. HIF has been found to promote cell differentiation by activating the expression of genes encoding glycolytic enzymes (32).

1.3.4 Glutamate and glutamine

Glutamate, the primary excitatory neurotransmitter in the mammalian brain, serves as the direct precursor for γ-Aminobutyric acid (GABA). Furthermore, glutamate plays a crucial role in the formation of other small metabolites, such as glutathione(33, 34). It can be found at an average

concentration of 8-12 mM, indicating its significant presence and potential role in various metabolic processes in the brain (35).

Glutamine, primarily located in astroglia at a concentration of 2-4 mM, is derived from glutamate via the enzymatic action of glutamine synthetase within astroglial cells (36). It is further metabolized back into glutamate by phosphate-activated glutaminase, which is refer to as glutamine-glutamate cycle (33). As a key component of intermediary metabolism, glutamine has been implicated as a fuel source for a number of cancers (37).

Vital to the understanding, as glutamine is hydrolyzed by glutaminase to produce glutamate, Glutamate is subsequently converted to α-ketoglutarate making it an intermediate in tricarboxylic acid (TCA) cycle and an emerging as a hallmark of cellular energy.

1.3.5 Taurine

While the precise role of taurine remains elusive, it is postulated to function as an osmoregulator and potentially modulate the effects of neurotransmitters (38, 39). Taurine is ubiquitously present within all cells of the central nervous system with an approximate concentration around 1.5 mM (40).

1.3.6 Creatine

Creatine and phosphocreatine, collectively referred to as "total creatine," are found in both neuronal and glial cells and are integral to cellular energy metabolism. Creatine is believed to serve as an intracellular ATP buffer through its phosphorylation in proximity to ATP production sites by mitochondrial creatine kinase (MtCK), resulting in the formation of phosphocreatine (41). The normal concentration of creatine is around 8.83 ± 1.32 mM (42).

1.4 Available techniques in quantifying metabolites changes in gliomas

One widely used technique in quantifying metabolite concentrations in gliomas in a clinical setting is single-voxel (two-dimensional) magnetic resonance spectroscopy (43). However, there are a few limitations of this technique. One limitation is restricted coverage of the entire tumo,r which leads to incomplete sampling of the tumor volume. One the other hand, a large single voxel might include areas of necrosis/edema/normal brain which could influence the metabolic concentration in that captured voxel (44). Another major limiting factor especially for infiltrating glioma, is the inability to capture tumor cells or the metabolic changes that results from infiltrating tumor cells beyond contrast-enhancing region (45, 46) .All these limitations led to the introduction of other techniques one of which is three-dimensional echoplanar spectroscopic imaging (3D EPSI). This emerging modality maps the metabolites in a wide extent of the brain, including deep brain structures and cortical surface regions (47). By generating high-resolution, volumetric maps of metabolites, encompassing both supratentorial and infratentorial brain regions. Three-dimensional echo planar spectroscopic imaging can be spatially aligned with anatomical images, enhancing our ability to track variations in metabolite levels within normal brain parenchyma as well as tumor's actual spatial extent (48). Further, the approach of whole-brain data acquisition employed by 3D EPSI circumvents the issues of subjectivity and user bias associated with voxel placement.

Previous studies (49, 50) looked into the metabolic alterations associated IDH mutation mainly through a single-voxel spectroscopy (SVS). However, the global changes in brain metabolites driven by the mutation are still unclear. And the impact of these findings on clinical practice

including extent of resection or response to therapy is a promising application of this modality of imaging.

1.5 Peritumoral area

Early studies showed that up to 70–90% of recurrent glioblastoma occurred within 2–3 cm of tumor margin (51). Histological studies were able to identify invasive glioma cells at a greater distance from the primary tumor margin (52). Radiologically, some would define peritumoral area as the brain area surrounding the tumor contrast enhancement in T1 gadolinium-enhanced 3-dimensional magnetic resonance imaging (3D-MRI) (53). Zatterling et al (54), by coregistration histopathological and magnetic resonance imaging data concluded that tumor cells were found outside the radiological tumor border delineated on T2-FLAIR MRI sequences. Pallud et al (55), in the context of diffuse low-grade gliomas, analyzed serial stereotactic biopsies for untreated supratentorial well-defined and non-contrast-enhanced lesions in 16 adult patients. The study showed tumor cells at distances of 10 to 20 mm beyond the hypersignal areas on T2-weighted and FLAIR MRI sequences.

Although peritumoral area in glioma shares the same macroscopic aspect as the normal parenchyma. Peritumoral area has its own cellular characteristics. This includes infiltrating tumor cells, reactive astrocytes that been shown to promote tumor growth and survival, inflammatory cells particularly tumor-associated macrophages (TAMs), microglia, and other glioblastoma-associated stromal cells (GASCs) (53).

This raises the question as to how IDH mutation would impact the peritumoral area. Mortazavi et al (56), investigated IDH-mutant glioma-related epileptogenesis. Authors suggest that seizures are related to metabolic disruptions in the surrounding cortex secondary to 2-HG and its role in

TCA cycle and generation of hypermetabolic phenotypes. In another study using Mass spectrometry imaging to analyze tissue from IDH wild-type gliomas found that enhanced levels in lactate, glutamine in tumoral area with lower levels of NAA compared to peritumoral area. Additional investigation is warranted to better understand the influence of IDH mutations and the accumulation of 2HG on the peritumoral region.

1.6 Markers of tumor border

The delineation of tumor margins, particularly in non-contrast enhancing gliomas, remains a challenge. One proposed marker is lactate-to-N-acetyl-aspartate ratio (Lac/NAA) ratio. Deviers et al (57), demonstrated a Lac/NAA $\geq$ 0.4 would differentiate between tumor and normal values with 88.8% sensitivity and 97.6% specificity (findings not stratified by IDH mutation status). Choline/N-acetyl-aspartate (Cho/NAA) ratio was also suggested as higher Cho/NAA ratios were associated with a greater probability of higher MIB-1 counts, stronger CD34 expression, and tumor infiltration (58). In an interesting study conducted by Yan et al(59), authors generated spectroscopic quantification on glioma animal models looking into peritumoral area for possible markers. taurine was significantly lower in tumor periphery while, the glutamate and glutamine (Glx) concentration peaked at the tumor periphery. In this study we aim for a more in-depth exploration of choline, glutamate and glutamine in relation to IDH mutation status.

1.7 Global Metabolic changes driven by IDH mutation

Whole brain spectroscopy provides a unique opportunity to understand the spatial distribution of the disease as well as global metabolic reprograming beyond its local spread (60). Since the recent introduction of Whole-Brain 3D spectroscopic imaging into the field of glioma research,

few studies have explored its clinical potential. One way is the proposed tumor mapping based on 2 HG concertation (61). Other authors have utilized whole brain Echo-planar spectroscopic imaging by defining contralateral hemisphere as a control to compare tumoral metabolites (62). To our knowledge, no study has surveyed the metabolite levels in IDH glioma contralateral hemisphere and compared it to healthy brain. This study attempts to analyze the global impact of IDH mutant glioma by analyzing metabolites in the contralateral hemisphere.

1.8 Post-operative metabolic changes

For MRS studies to be effective, especially in cases suspecting glioma regrowth, it is vital to identify the patterns of change in metabolites between preoperative and postoperative MRS investigations. Correlating these alterations with clinical data regarding the progression of the disease can provide valuable insights. Czernicki et al (63), used one-dimensional voxel spectroscopy at the tumour resection site 6 month post-operatively. Authors concluded that an increase in Cho/NAA ratio and decrease in NAA/Cr ratio, is suggestive of glioma regrowth rather than post-radiation cerebral necrosis. Andronesi (64) et al, measured 2HG levels in IDH-mutant glioma patients receiving adjuvant radiation and chemotherapy. Interestingly, mean 2HG levels decreased significantly by 48% in the post-treatment scan. Furthermore, decreased 2HG level was found to correlate with clinical status measured by Karnofsky Performance Scale (KPS).

In this study, we hypothesize that using whole brain MRSI will capture metabolic changes driven by IDH mutation within the tumoral and peritumoral regions. To achieve this, we sought to utilize whole brain spectroscopy to compare these areas to healthy control subjects and IDH wild-type tumors. Next, we sought to investigate the effect of IDH mutation status on global

brain metabolites by analyzing the contralateral side. Third, we explored metabolite alterations in the peritumoral area to identify markers of tumor boarder. Lastly, we sought to assess if cytoreduction achieved by surgical resection results in dynamic changes of peritumoral metabolites.

Chapter 2: Materials and Methods

2.1 Study design

A prospective longitudinal observational study was conducted at the Montreal Neurological Institute, Montreal, Canada from March 2022 to May 2023. The study was approved by the McGill University Health Centre Research Ethics Board Neurosciences and Psychiatry panel (REB# 2019-5455). We recruited patients with suspected WHO grade II-IV IDH mutant glioma at diagnosis or suspected recurrent WHO grade II-IV IDH mutant glioma who are scheduled to undergo open surgical resection. At the time of recruitment IDH mutation status was known or will be established following surgery as per standard clinical practice. Post-operative scans were conducted at 2 weeks mark.

The following clinical data was collected at the time of enrolment (age at the time of scan, age at diagnosis, sex, prior radiation or chemotherapy, dose of Decadron at the time of imaging, seizure history before and after surgery, antiepileptic medication use, histological diagnosis and tumor grade, IDH mutation status)

2.2 Magnetic Resonance Spectroscopy Imaging (MRSI) Acquisition:

All MRI and MRS scans were performed on one 3.0T MRI scanner in collaboration with The McConnell Brain Imaging Centre. Acquisition of each scan required 75 minutes.

2.2.1 Parameters used for EPSI

Delta frequency: -2.20 ppm, Phase encoding: Elliptical, Bandwidth: 125000 Hz

Acquisition duration: 8 ms, Vectors: 512, TE 17.1

2.2.2 Parameters used for fluid attenuated inversion recovery (FLAIR)

1-mm-thick 2D clinical FLAIR images were acquired for anatomical correlation. The acquisition also obtained a water-reference SI dataset.

2.3 Imaging Processing

MIDAS (Metabolic Imaging Data Analysis System) software package was used for processing, display, and analysis of MR Spectroscopic imaging data. MIDAS software supports a volumetric echo- planar spectroscopic imaging (EPSI) acquisition and display a high-resolution map of the brain, including cortical surface regions. Processing included linear registration calibration between T1-weighted MR and whole-brain MRSI. Detection of metabolic maps conducted from the water reference MRSI with a voxel volume of 1.55 cc

All processing parameters are predefined. These include.

- Four-Dimensional Fourier Transform (FDFT) which performs dimensional transformation along with several standard MR signal processing operations to generate multidimensional spectroscopic imaging data
- Automated spectral fitting of single spectra (FITT), fitting is conducted based on parametric modeling generated from established prior knowledge of the metabolite resonances
- METAFIT, enable fitting on low metabolic signals such as glutamate and lactate.
- Volumizer organizes data in a consistent way following importing of raw images prior data processing

- Pre-Processing for EPSI Data (EPSI2) converts (spectroscopic imaging) SI data acquired with an echo-planar readout into the Cartesian data organization that are used for processing
- Reference MRSI Data Formation (REFDAT) creates a reference to obtain correction functions for the spectral processing performed through FDFT step.

2.4 Imaging Analysis

2.4.1 Regions of interest (ROI):

Tumoral (ROI): Created based on FLAIR hyperintensity

Peritumoral area (pROI): Defined to include 1 cm band around the ROI

Contralateral brain (cROI): estimated on the midsagittal plane of the brain on T1w of the contralateral brain hemisphere, volume was selected as a contiguous WM region in the supraventricular region of the brain (top 6 cm of the brain)

Post-operative (post-opROI): included 1 cm band around surgical bed margins

2.4.2 Segmentation

Raw Digital Imaging and Communications in Medicine (DICOM) MRI data of 1 mm FLAIR images were imported into 3D Slicer software where a manual segmentation was performed to define each region of interest (ROI) which is created based on FLAIR hyperintensity signal. Peritumoral area (pROI) was defined to include 1 cm band around the ROI (Figure.1)

2.4.3 Spectrum fitting

Fitting is then conducted on each region of interest (ROI) to generate a spectrum by integrating multiple voxels. Heatmaps metabolite images are reconstructed from automated spectral fitting of the volumetric MRSI data (Figure 2)

2.4.4 Heatmaps

MRIcroGL was used to map analyzed DICOM data from MIDAS after converting them to NIfTI format image to view different overlays. Overlays were adjusted manually to intensity range values and the color scheme to emphasize different tissues

2.5 Statistical analysis

The mean regional Cho, Cr, Lac, NAA, GLX, Glu, Gln, LAC/NAA, Cho/NAA for 26 regions of interested were corelated using student t-test and One-way ANOVA to test for differences in metabolite concentrations among the different areas. All procedures were carried out using SPSS version 17 for Windows (SPSS Inc., Chicago, IL, USA). P-value (q) less than 0.05 was considered significant for the correlations.

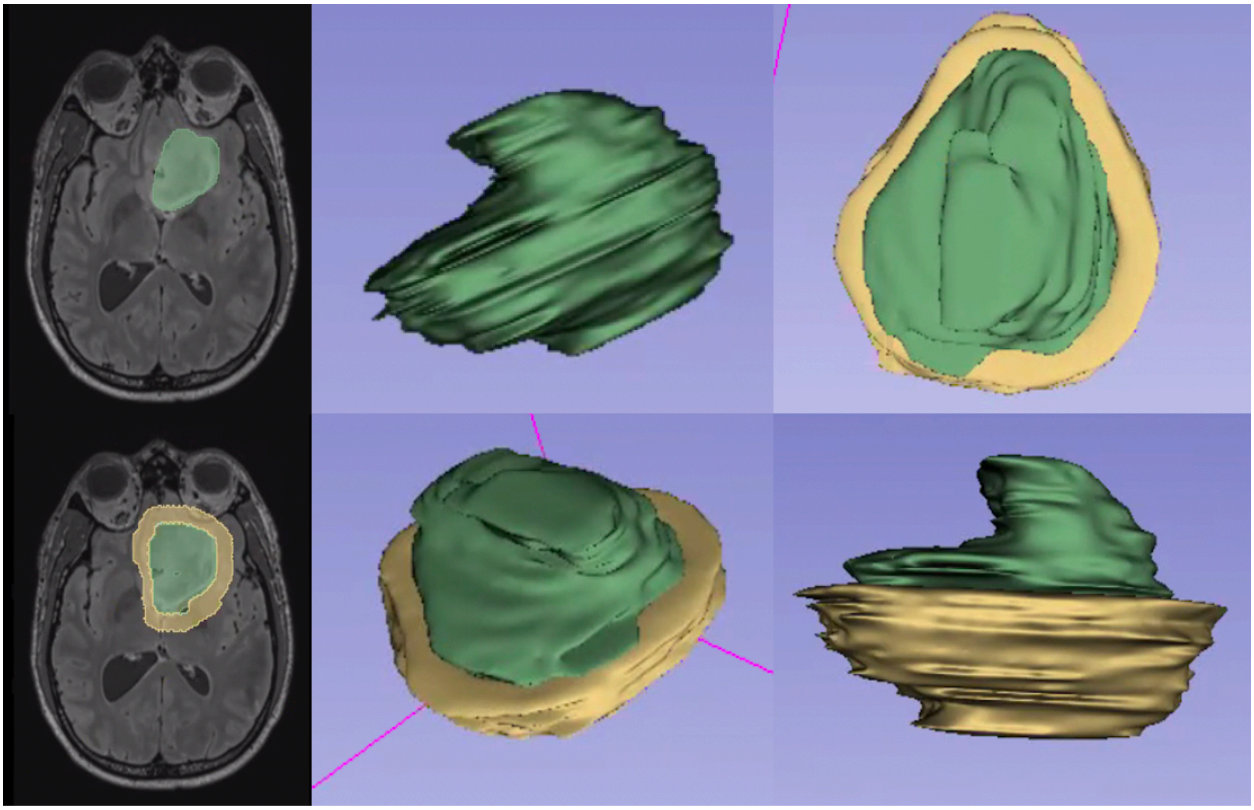

Figure.1: Multiple views demonstrating segmentation analysis manually performed on both tumor and peritumoral areal

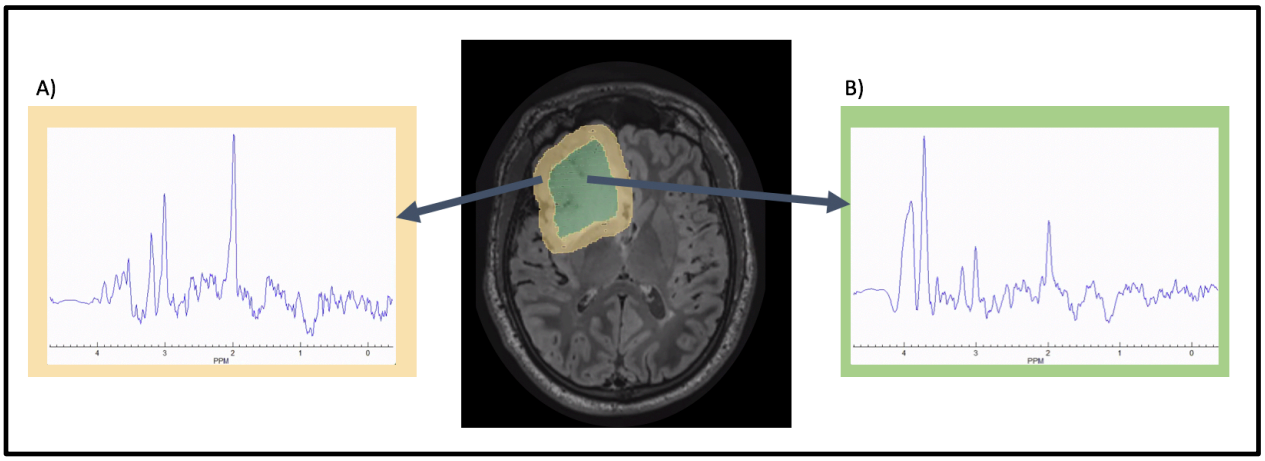

Figure.2: One fitted spectrum is generated by integrating multiple voxels of the defined region of interest (ROI). In this example A: represent the spectrum for peritumoral area while B: the spectrum represents tumoral area.

Chapter 3: Results

3.1 Study population

We recruited a total of 8 patients (5 IDH mutant and 3 IDH Wildtype) as well as 4 adult healthy control. Among IDH mutant patients four were males and one was a female. Four had frontal lobe occupying tumors and one had frontotemporal tumor. Post-operative images were obtained for three patients (#1,#3,#4) Patient #2 required a long rehab center admission, patient #5 pending available scanning time from McConnell Brain Imaging Centre. IDH-wild type group included two females and one male. Anatomical distribution of the tumor varied to include frontotemporal, temporoparietal and parietooccipital. Post-operative images were obtained for one patient (Patient#2). Patient#1 had multiple post-operative comorbidities resulted in bedridden status, while Patient#3 is pending available scanning time from McConnell Brain Imaging Centre. We aimed for two weeks post-operatively to obtain the scans. Given scanning time availability, mean waiting time was 32.5 days. Two patients (#4, #2) were on adjuvant therapy while obtaining the scan including radiotherapy and temozolomide.

Table.1 demonstrating the clinical characteristics for IDH mutant and IDH wild-type patients as well as the healthy control volunteers.

Subject	Sex	Age at the time of diagnosis	Location	Mutation status
1	M	33		
2	M	33	N/A	Healthy Control
3	F	34		
4	F	30		
1	F	64	Rt Frontotemporal	
2	F	58	Rt Temporoparietal	IDH Wild-type
3	M	36	Lt parietooccipital	
1	M	45	Lt Frontal	
2	M	33	Rt frontal	
3	F	28	Lt frontal	IDH Mutant
4	M	25	Rt frontotemporal	
5	M	30	Rt Frontal	

3.2 Characterization of IDH mutant tumoral area

To study the effect of IDH mutation on brain metabolites, we compared the mean of each metabolite of interest found in the five IDH mutant tumors to four healthy controls. Choline was found to be elevated in all five subjects when compared to healthy control (P=0.044). NAA in the other hand was markedly lower in all subjects in relation to the healthy control (P=0.040). Creatinine was relatively reduced but with variability across IDH mutant patients.

To test the value of measuring metabolites ratios in identifying tumoral area, both Cho/NAA (2.3671 vs 0.0957) and Lac/NAA (1.4102 vs 0.1867) were higher in IDH mutant glioma when compared to healthy control (P=0.0001).

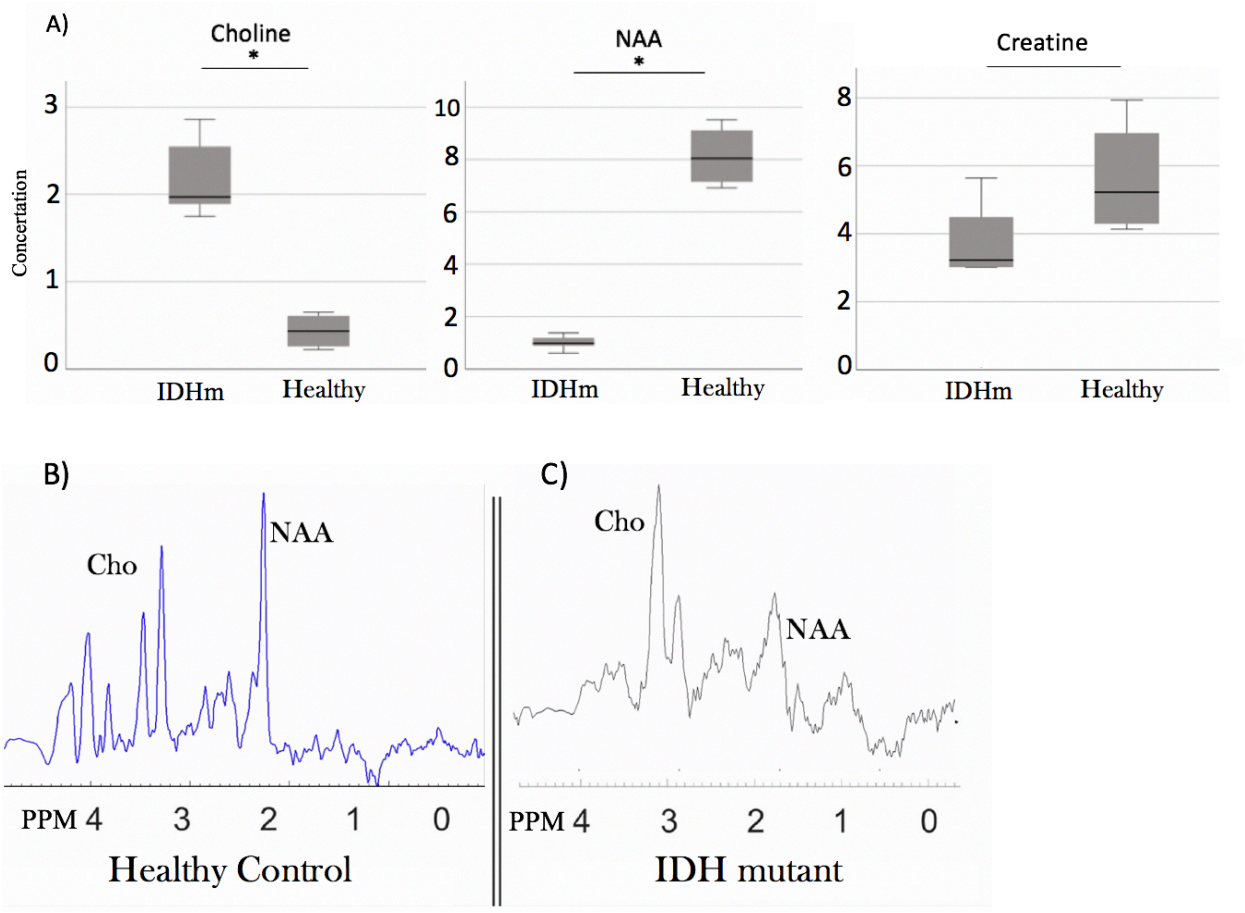

Figure.3: A) Choline (Cho), Creatine (Cr), and N-Acetyl aspartic acid (NAA) concentrations in four healthy control compared to five IDH mutant areas. An asterisk indicates a statistically significant difference. B) An average spectrum from a healthy control is demonstrated. C) Fitted spectrum of a tumoral area of Patient#4 showing higher levels of choline and lower levels of NAA in IDH mutant area compared to the healthy control. Concentrations measured by millimolar (mM). The methyl protons of choline-containing compounds at circa 3.2 ppm while NAA resonance originates from the methyl group of NAA at 2.01 ppm.

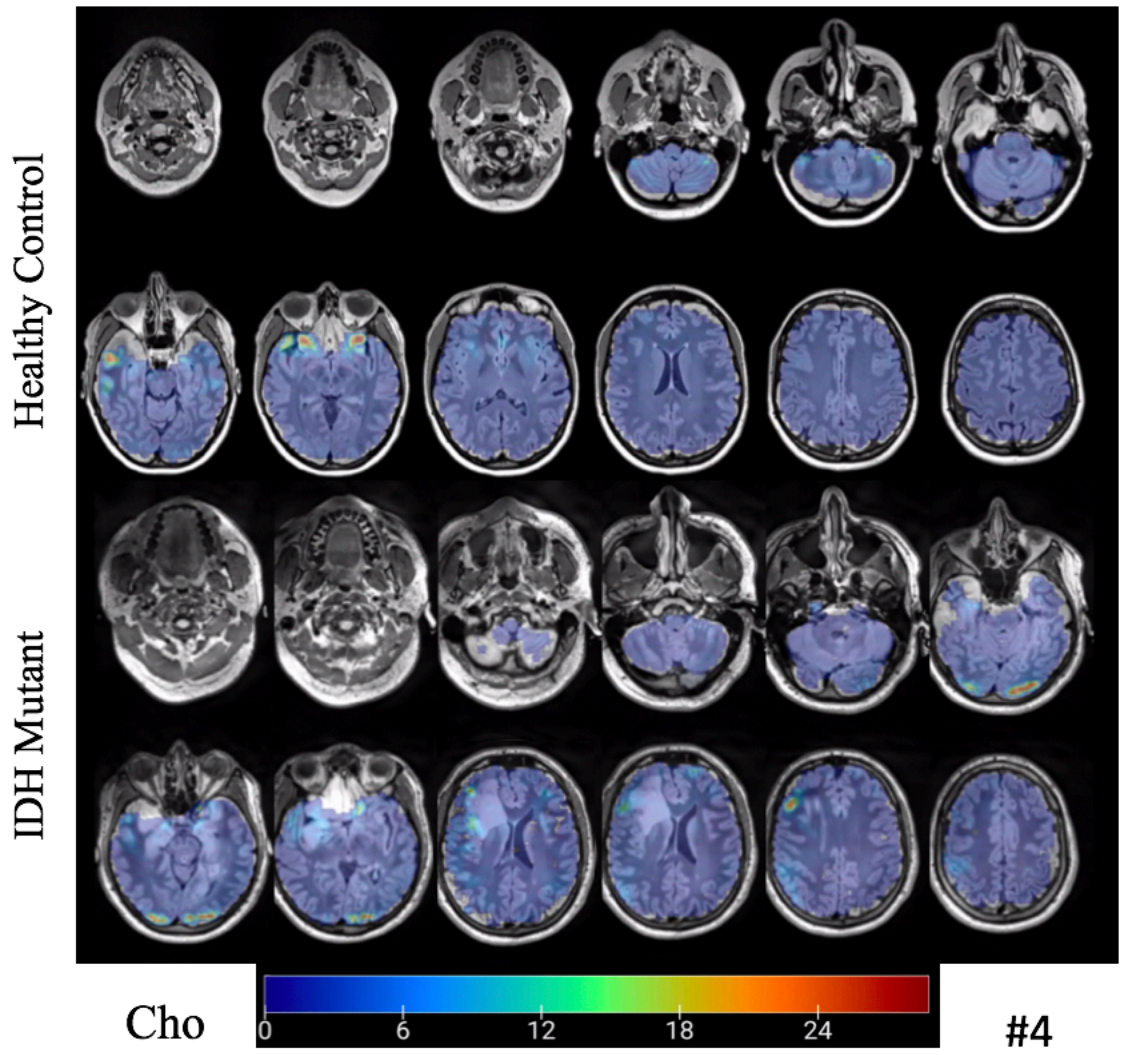

Figure.4 Heatmap images of axial T1 images overlayed with whole brain metabolic map of Choline comparing the concentration between a healthy control subject#3 and IDH mutant patient#4. Brighter signal picked up across the tumoral area indicating higher levels of Choline.

3.3 IDH mutant tumoral area compromise a distinct metabolic profile in relation to IDH wildtype

To test the hypothesis that IDH mutation impact metabolic distribution in the tumoral area, we compared the mean of each metabolite of interest in the five IDH mutant tumors to IDH wild type three subjects. One main finding is the elevated Cho levels observed in IDH mutant tumor compared to wildtype (P=0.0001). Interestingly, Lac was significantly higher in IDH wild type in relation to IDH mutant tumors.

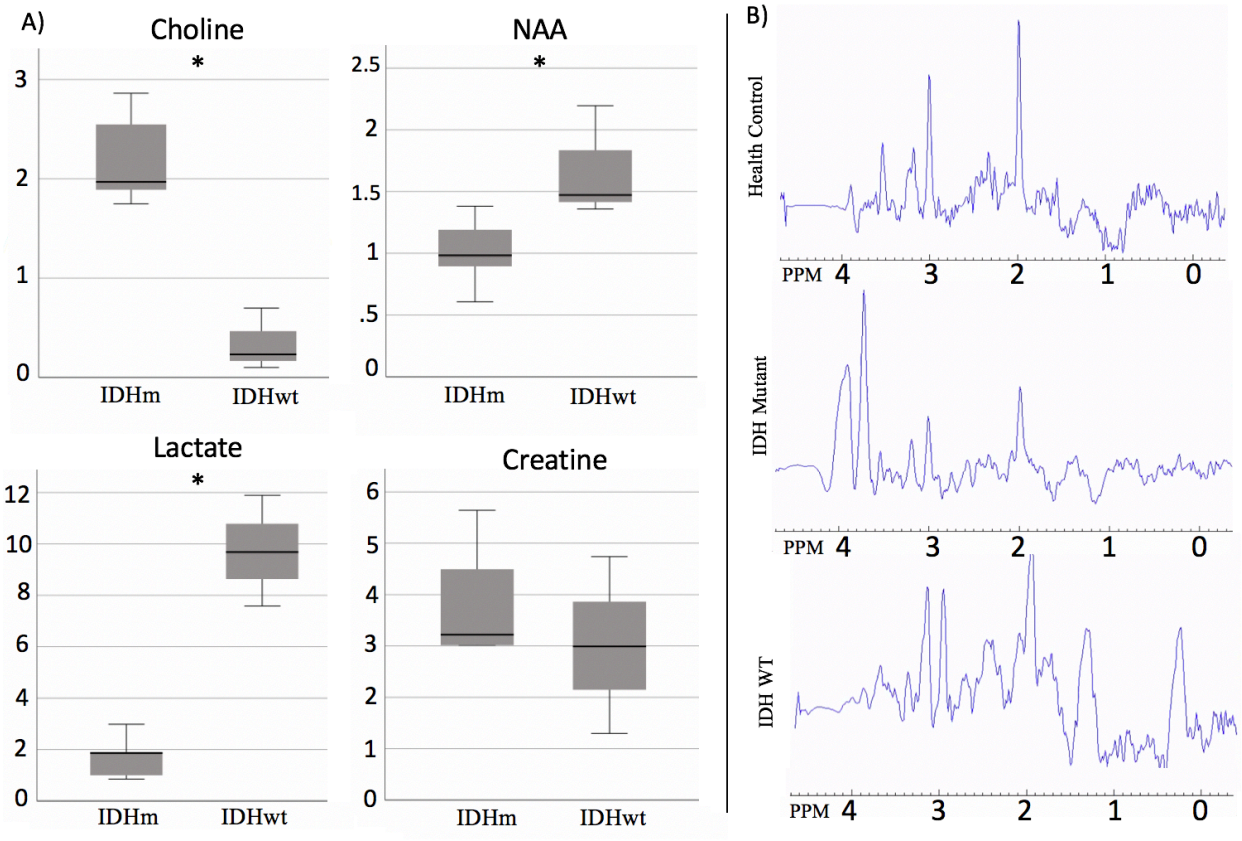

Figure.5: Boxplot showing A) Choline (Cho), N-Acetyl aspartic acid (NAA), Creatine (Cr), and Lactate (Lac) concentrations five IDH mutant tumoral areas compared to three IDH wild-type tumoral areas. With significantly higher levels of Cho and lower levels of NAA in IDH tumoral areas while IDH wild-type showed higher levels of Lac. An asterisk indicates a statistically significant difference. B) Comparison of a spectrum from a healthy control, IDH mutant tumoral area (Patient#4) and a spectrum from IDH wild-type tumoral area (Pateint#3). Concentrations measured by millimolar (mM). An asterisk indicates a statistically significant difference. The methyl protons of choline-containing compounds at circa 3.2 ppm while NAA resonance originates from the methyl group of NAA at 2.01 ppm. Lactate at 1.3 ppm.

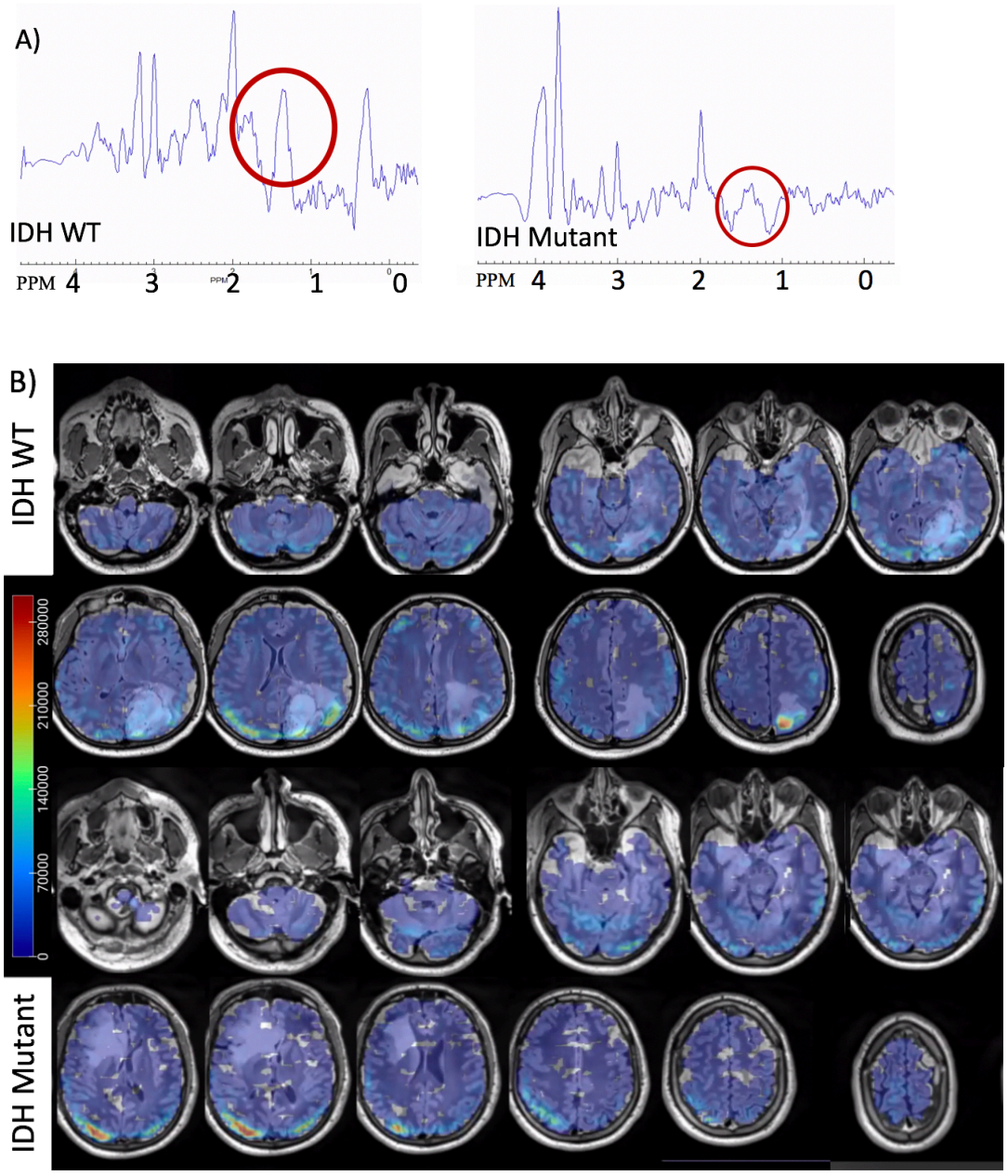

Figure.6: A) Fitted averaged spectrum indicating higher lactate resonance in IDH wild-type tumoral area compared to IDH mutant tumoral area. lactate resonance is present at signal at 1.31 ppm. B) Heatmap of axial T1 images overlayed with whole brain metabolic map of lactate showing higher signal in IDH wild-type vs mutant tumoral aeras.

3.4 Glutamine and Glutamate as a fuel source for cancer metabolism

To study the role that both Glutamine and Glutamate play in driving the metabolism in IDH mutant tumors, we quantified the concentrations of both in IDH mutant, wild type and healthy control. We noticed a drop in the concentration of glutamate with higher levels of glutamine were observed in IDH mutant tumors compared to healthy control (P=0.02). When compared to IDH wild type, IDH mutant tumors showed significant decrease in glutamate concentration (P=0.001).

Interestingly, compared to the healthy control peritumoral areas of IDH mutant had significantly reduction of glutamate (P=0.007). Although glutamine was not significantly different, overall GLX was lower in IDH mutant peritumoral area. However, IDH wild-type peritumoral area did not show significant finding in glutamate or GLX (P=1.02 and P=0.79)

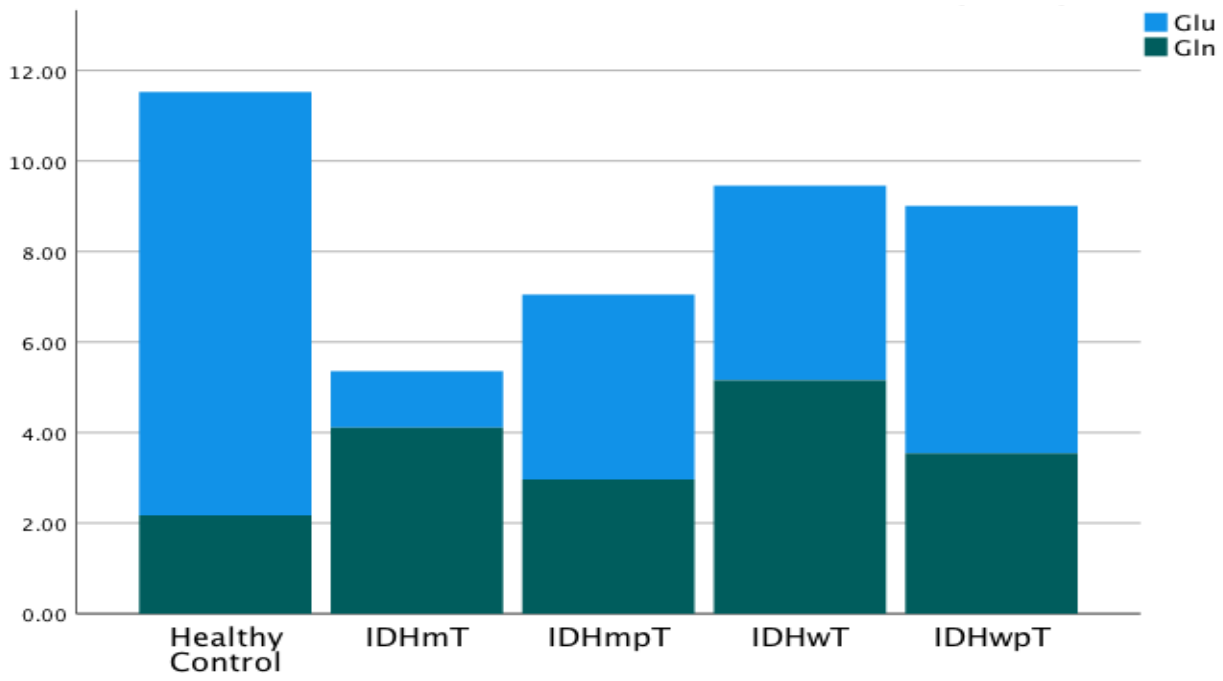

Figure.7: Stacked bar showing the mean concentration millimolar (mM) of (Glutamate (Glu), Glutamine (Gln) and GLX (Glu+Gln) for IDH mutant tumoral area (IDHmt), IDH mutant peritumoral area (IDHmpt), IDH wild-type tumoral area (IDHwt), IDH wild-type peritumoral area (IDHwpt) and healthy control. Significant drop of glutamate concentration noticed in IDH mutant tumoral area compared to IDH wild-type tumoral area and healthy control(P=0.001). Higher levels of glutamine were also observed in IDH mutant tumoral areas. These significant alterations in Glu and Gln were also seen in IDH peritumoral area when compared to the healthy control (p=0.0001) but not significantly evident in IDH wild-type peritumoral area.

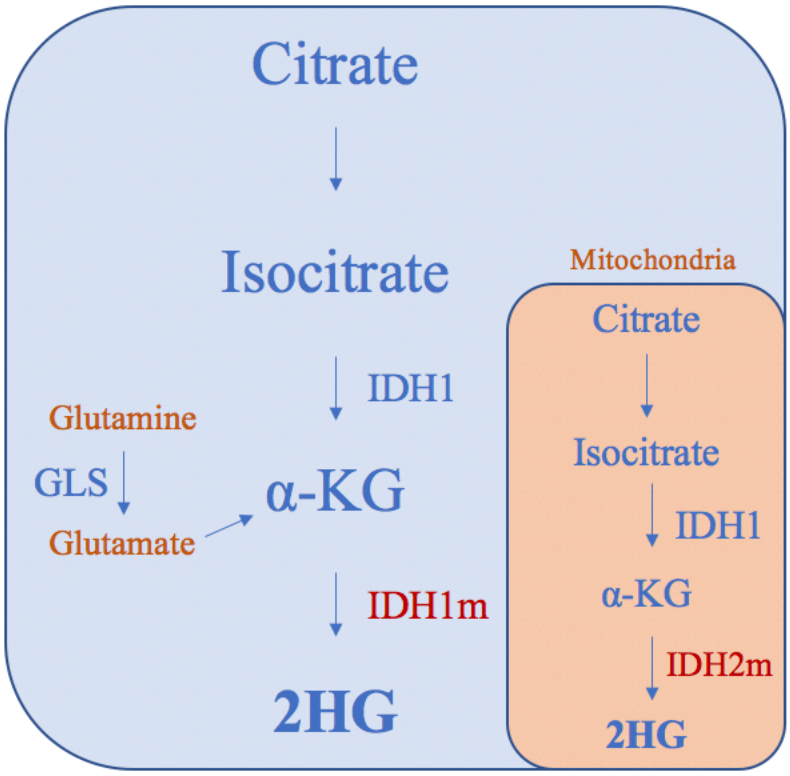

Figure.8: Illustration demonstrating the role both glutamine and glutamate play in the Krebs cycle metabolism. Glutamine is hydrolyzed by glutaminase to produce glutamate, which is subsequently converted to α-KG.

3.5 Peritumoral area and potential biomarkers indicating tumor border.

When comparing tumoral to peritumoral area of IDH mutant tumors, Cho and Tau and glutamine were higher in concertation in tumor vs peritumoral area (P=0.000, P=0.003 and P=0.02 respectively). Glutamate was significantly lower in IDH mutant tumoral area when compared to peritumoral area. Correlation Cho/NAA ratio was also higher at 2.1755 for tumor area vs 0.1789 for peritumoral area (P=0.001).

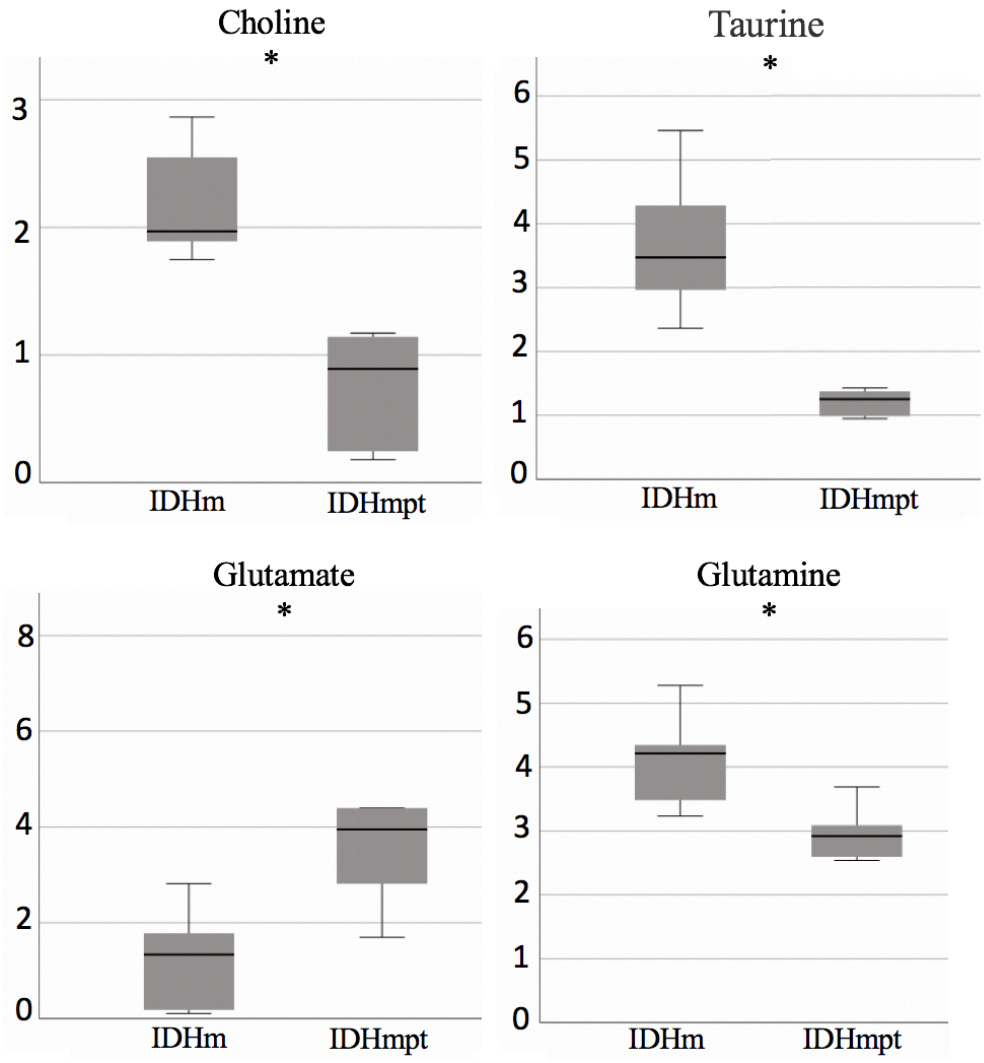

Figure.9: Showing potential biomarkers of tumor border with significant change between tumoral (IDHm) and peritumoral area (IDHmpt) among IDH mutant tumors. Concentrations measured by millimolar (mM). An asterisk indicates a statistically significant difference

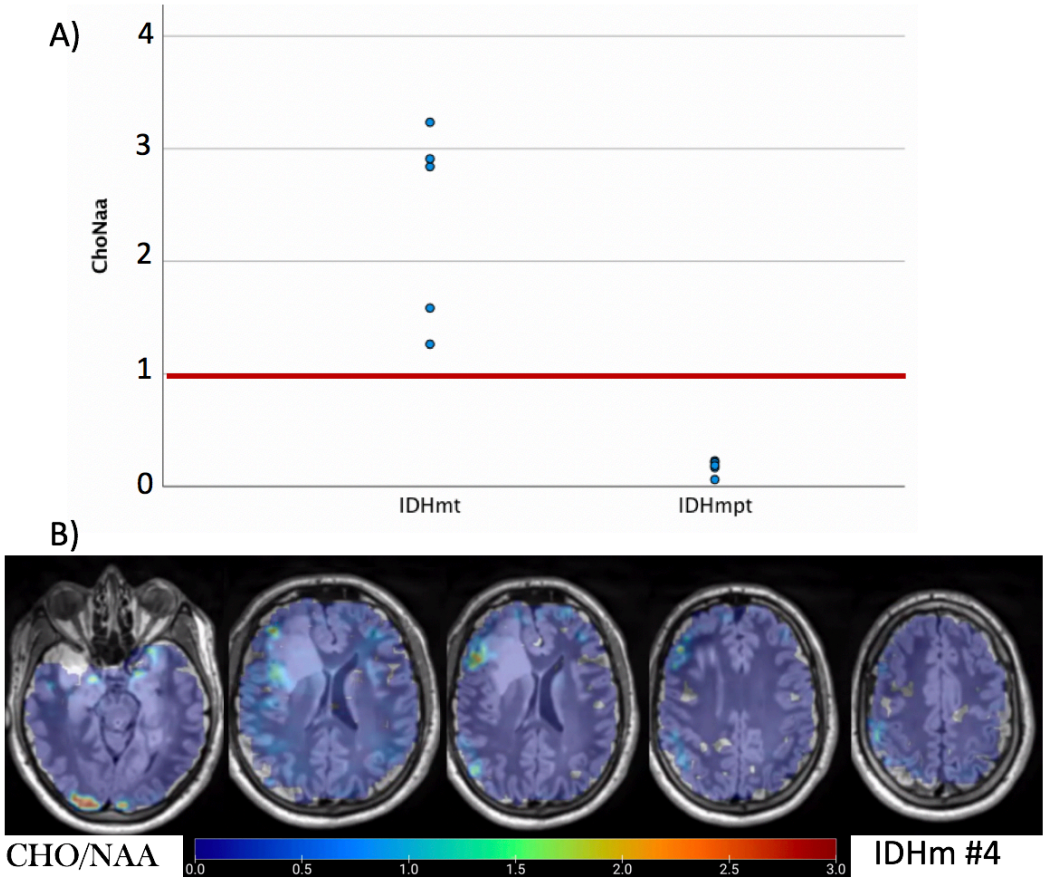

Figure.10 A) showing CHO/NAA correlation level that was significantly higher in IDH mutant tumoral area (IDHmt) when compared to peritumoral area (IDHmpt). Interestingly, all peritumoral CHO/NAA measurements fell below 1. B) Heatmap of axial T1 images overlayed with whole brain metabolic map of CHO/NAA, higher signal observed at the tumor compared to peritumoral area.

3.6 Post-operative analysis

To study the effect of surgical resection for IDH mutant tumors, we compared preoperative peritumoral area to post-operative peritumoral area. Only Glutamate (P=0.023) that was statistically different between the groups Choline (P=0.32), Creatine (P=0.54), Lactate (P= 0.25), NAA (P= 0.12), Glutamine (P=0.25). When comparing post-operative peritumoral area to Glutamate measurement to healthy control subjects, no significant change found (P=0.07). Cho/NAA showed lower values post operatively compared to preoperative peritumoral area 0.04 vs. 1.54 but not statistically significant (P=0.067)

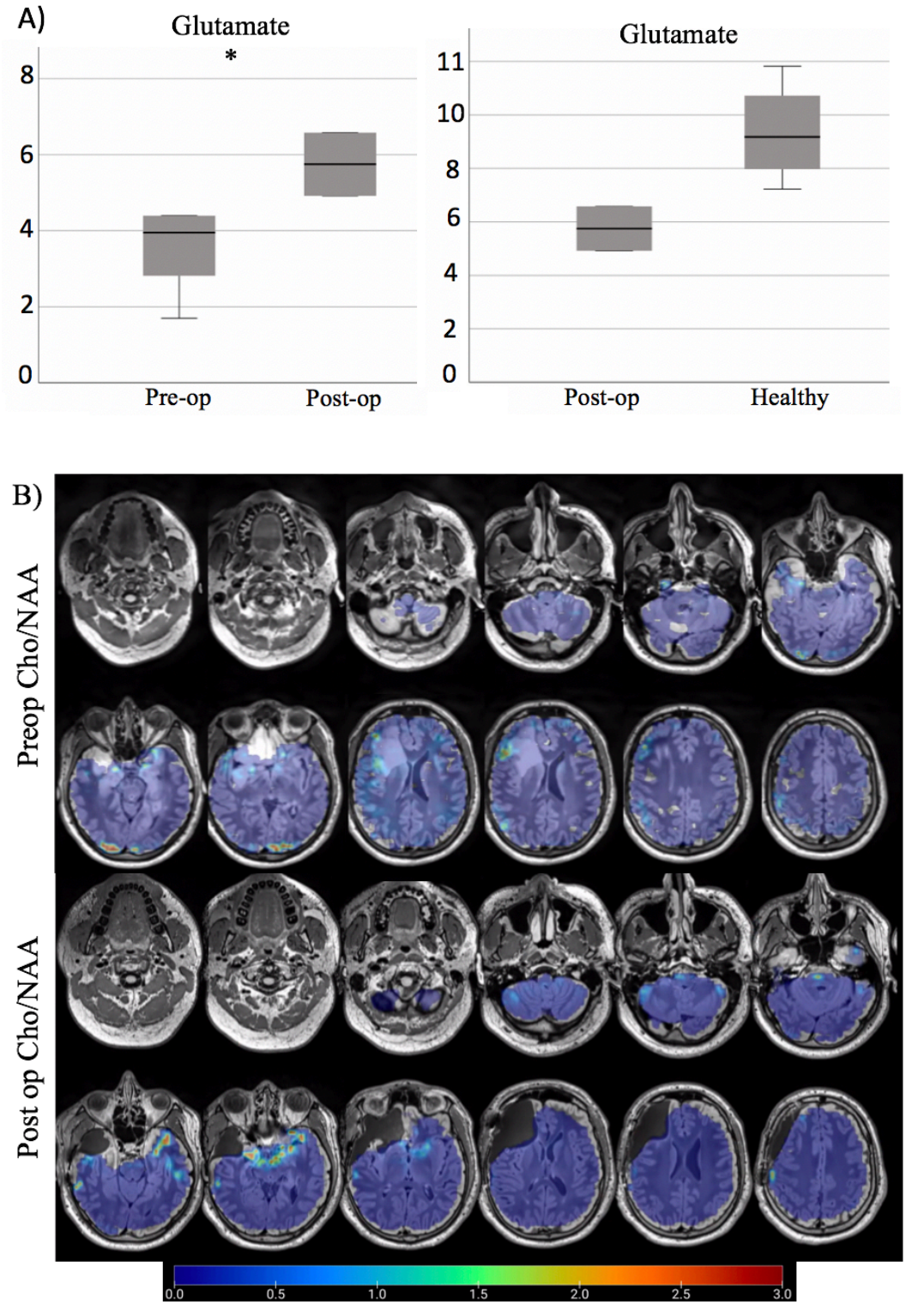

Figure.11 Post-operative analysis showing significantly elevated levels of glutamate in post-operative IDH mutant peritumoral area (post-op) when compared to pre-operative peritumoral

area (pre-op), No significant difference found between post-operative IDH mutant peritumoral area (post-op) and healthy control subjects. B) Heatmap of axial T1 images overlayed with whole brain metabolic map of CHO/NAA. Diminished signal is noticed in post-operative surgical bed. Concentrations measured by millimolar (mM). An asterisk indicates a statistically significant difference.

3.7 Global metabolic changes

To study the global metabolic changes, we measured metabolites concentration in contralateral hemisphere for both IDH mutant and IDH wild type gliomas. First, we compared (choline, NAA, Lactate, creatine, glutamine, glutamate) between IDH mutant contralateral area to the healthy control. No difference was found in individual metabolites of interest (P=0.45, P=0.07, P=0.03, P=0.63, P=0.60 and P=0.22 respectively). Second, we compared choline, NAA, Lactate, creatine, glutamine, glutamate) concentration in contralateral areas between IDH mutant and IDH wild type, no significant difference reported in different individual metabolite (P=0.14, P=0.25, P=0.35, P=0.55, P=0.92 and P=0.09 respectively).

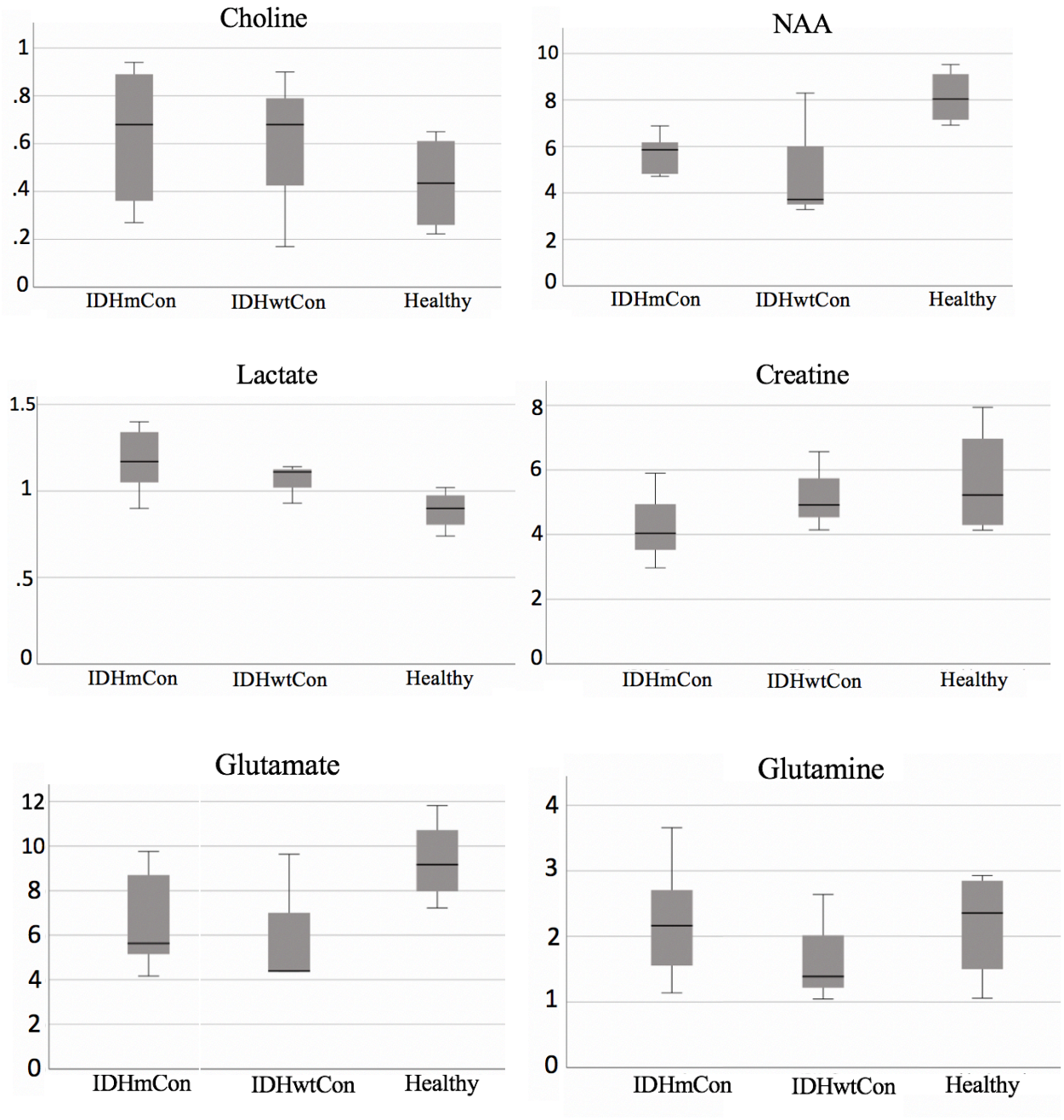

Figure.12 Comparison between IDH mutant contralateral area (IDHmCon), IDH wild-type contralateral area (IDHwtCon) and healthy control subjects showing no significant change in metabolites of interest including Choline, NAA, Lactate, Creatine, Glutamate and Glutamine

Chapter 4. Discussion

Whole brain three-dimensional spectroscopic imaging is a feasible tool to display metabolic reprogramming driven by IDH mutation (65, 66). We found multiple metabolites that were significantly different between IDH mutant and IDH wild-type tumoral areas and possibly altered as a result of the mutation. One of which is N-Acetylated Amino Acids (NAA) with a drop in concentration found in IDH mutant tumoral area compared to both healthy control subjects and IDH wild-type tumoral area. One possible explanation, supported by Reitman *et al* (67), is the IDH mutation mediated downregulation of *N*-acetyltransferase enzymes or the upregulation of breakdown of *N*-acetylated amino acids. Although this phenomenon is not fully understood, Reitman *et al* found low levels of acetyl-CoA (substrates for *N*-acetyltransferase) associated with low levels of *N*-acetylated amino acids in glioma cells expressing IDH1 or IDH2 mutants. Another possible explanation is the depletion of glutamate. Glutamate is a substrate for *N*-acetyl-aspartyl-glutamate (NAAG) synthetase which is part of the N-Acetylated amino acids compound (67).

Choline has been used as marker of cellular density as it reflects cellular membrane turnover (26). Interestingly, we found elevated choline concentration not only in comparison with the healthy control, but also in relation to IDH wild-type. Furthermore, elevated Choline levels were also seen IDH mutant peritumoral area. In 1999 prior to the IDH mutation-based classification, Sabatier *et al* (68), studied choline concentration using in vitro magnetic resonance spectroscopy. Authors found higher levels of choline in low-grade astrocytomas compared to high grade. In the study, authors suggested that these finding could be a result of organized membrane proliferation

while the lower choline levels detected in high grade glioma might be related to the necrotic nature of these tumors.

To understand the correlation between choline concentration and IDH mutation, it is important to highlight the relationship between 2HG and cellularity. Jalbert *et al* (69), investigated the metabolic profiles of *ex vivo* IDH mutant glioma cells. They found a correlations between 2HG levels and mitotic activity (measured by MIB1 antibody staining). Similar results were reported by Pope *et al* (70) were 2HG levels were correlated with the Ki-67 proliferation index of the IDH mutant tumors. These findings indicate an increase in cellularity linked to the production of 2HG, and potentially suggest choline to serve as an in vivo biomarker IDH mutant glioma.

Correlation levels have been suggested to differentiate tumoral voxels from normal voxels. One proposed parameter is Cho/NAA ratio which has further been suggested as a biomarker of tumor prognosis and treatment response. Bulik *et al (71),*suggested a Cho/NAA ratio of ≥1.4 to differentiate recurrence from pseudoprogression. Furthermore, Cui *et al* (72) recently suggested Cho/NAA ≥ 1.31 in peritumoral area was as an independent risk factor for early recurrence, however only (9.0%) of their cohort harbored IDH mutation. In our study, Cho/NAA ratio was markedly higher in tumoral area when compared to healthy control. Interestingly IDH mutant tumoral area had a higher ratio (all >1) when compared to peritumoral area which could indicate a higher cellular proliferation driven by IDH mutation. Which could also be implemented as a marker of tumor border.

Glutamate/ Glutamine cycle is a critical element in brain metabolism. By serving as an important excitatory neurotransmitter, glutamate is critical for glutamatergic neurons synaptic cleft and

therefore multiple brain functions (73). Astrocytes sustain glutamate homeostasis by eliminating glutamate toxicity through glutamate/ glutamine neuroglial cycle (33). This process is hijacked by tumor cells. It has been shown that glioma cells compete for the glutamine to promote their proliferation. One possible mechanism is by upregulating expression of glutamine and glutamate importers such as ASCT2 (SLC1A5) SNAT3 and SNAT-5. As a result, rapid of glutamine influx is redirected toward the tumor microenvironment (74).

In IDH1-mutated gliomas, further alterations in Glutamate/ Glutamine is expected, given their contribution in TCA cycle. One study looked into TCA cycle intermediates in mutant IDH1- and IDH2-expressing cells (67). They found elevated flux from glutamine to 2HG related to IDH1-R132H expression. Furthermore, depletion of glutamate as it is converted to α-ketoglutarate and then to 2HG (Figure.7).

In our study, depletion of glutamate and increase of glutamine seen in IDH mutant and IDH wild-type tumoral areas is suggestive of the high energy demand required to maintain tumor growth and proliferation. Interestingly, IDH mutant tumoral area showed significantly higher concentration of glutamine and lower concentration of glutamate when compared to IDH wild-type. These results suggest glutamine-to-glutamate conversion as a metabolic hallmark for IDH-mutated cells.

Interestingly, IDH wild-type tumoral area showed higher concentration of lactate compared to IDH mutant area. As the end-product of nonoxidative glycolysis, lactate has been shown to reflect hypoxic environments(75). Few recent studies have investigated the association of IDH mutation and multiple glycolytic factors. Koivunen *et al* (76), demonstrated downregulation of HIF-1α driven by 2-hydroxyglutarate. Chesnelong *et al* (77), was the first to report

downregulation of lactate dehydrogenase by 2-hydroxyglutarate in IDH mutant cells. Lactate dehydrogenase is essential for glycolysis as it convert pyruvate to lactate. An IDH mutation-dependent silencing of lactate dehydrogenase might reflect a limited glycolytic capacity in IDH mutant glioma, which might explain the better prognosis in IDH mutant compared to IDH wildtype glioma. In accordance with these findings, our results showing a reduction in lactate concentration in IDH mutant tumoral area might offer a potential tool for prognostication in patients with glioma

Given that the prognosis for patients with high-grade gliomas is largely contingent on the extent of tumor resection, the development of innovative imaging techniques for accurately determining tumor margins preoperatively is crucial. One unique feature in whole-brain spectroscopy is the ability to study peritumoral area for possible biomarkers for tumor border.
In our study, although Cho was higher in IDH mutant tumors tumoral and peritumoral areas, a marked drop was noticed between the two areas. Maudsley *et al* (78), in their analysis of peritumoral area found an increase in Cho ratios in the peritumoral regions of IDH mutant tumors when compared to IDH wild-type, Together these findings suggest Cho as a marker for tumor border especially in IDH mutant tumors

Another interesting finding is the drop of Tau (which is known for its osmoregulation function) in IDH mutant peritumoral area compared to IDH mutant tumoral area. One possible hypothesis is that Tau has a higher water solubility than other metabolites and an increase in interstitial water in peritumoral area will lead to dramatic fall in its concentration (59). Other proposed

biomarker were glutamate and glutamine that showed significant difference in concentrations between IDH tumoral area and peritumoral area. These changes are likely related to increase energy demand within the tumor.

Post-operative analysis of IDH mutant peritumoral area showed marked increase of glutamate concentration, these findings suggest an initial metabolic recovery as a result of alleviating tumor mass. Future research corelating post-operative glutamate concentration to progression free survival and overall survival is a potential tool in our prognostication of IDH mutant gliomas

Few studies have looked into the contralateral area as a control to investigate global metabolic changes induced by gliomas. To our knowledge this is the first model used to compare both IDH mutant and wildtype contralateral areas to healthy control. In 2009, one study (79) performed single-voxel MR spectroscopy to compare high grade glioma (HGG) and low grade glioma (LGG) contralateral hemisphere to healthy control subjects. There were no significant differences between LGG and control subjects, while HGG had increased concentrations of myo-inositol and glutamine. IDH mutation status however was not defined in the study.
In our study no significant difference in individual metabolites of interest were found between IDH mutant or IDH wildtype contralateral areas and healthy control subjects. Our findings suggest that although metabolic alterations driven by IDH mutation reach beyond the FLAIR signal into peritumoral area, no global impact is captured secondary to the mutation.

Limitations of this study include the ability to accurately quantify 2-HG. A short TE acquisition of 17.6 milliseconds has been used to optimize glutamate and glutamine detection, however

measuring 2-HG would require a long TE (120—288 ms). Heatmap reconstruction from EPSI sequence is associated artifact adjacent to bony structure such as tumors close to the skull base. To avoid the inclusion of low-quality spectroscopic data, an automatic quality assurance procedure is used as part of the MIDAS programming. Another limitation was recruitment of IDH wildtype patients given their rapid clinical deterioration which precluded the opportunity to scan prior to surgical resection.

In conclusion, whole brain spectroscopy provides a unique opportunity to investigate metabolic reprogramming driven by IDH mutation. An increase in choline, glutamine with a reduction of glutamate reflect an IDH-mediated increase in cellular density with higher energy demand captured in these tumors. Furthermore, understanding peritumoral area as a specific entity could provide a promising tool for pre-operative mapping such as choline, taurine, glutamine and glutamate. Finally, our results indicate that while the metabolic changes triggered by IDH mutations extend beyond the FLAIR signal into the peritumoral region, these alterations do not appear to have a global impact attributable to the mutation.

Chapter 5. References

1. Sebök M, van Niftrik CHB, Muscas G, Pangalu A, Seystahl K, Weller M, et al. Hypermetabolism and impaired cerebrovascular reactivity beyond the standard MRI-identified tumor border indicate diffuse glioma extended tissue infiltration. Neurooncol Adv. 2021;3(1):vdab048.
2. Jackson C, Choi J, Khalafallah AM, Price C, Bettegowda C, Lim M, et al. A systematic review and meta-analysis of supratotal versus gross total resection for glioblastoma. J Neurooncol. 2020;148(3):419-31.
3. Zeng Q, Ling C, Shi F, Dong F, Jiang B, Zhang J. Glioma infiltration sign on high b-value diffusion-weighted imaging in gliomas and its prognostic value. J Magn Reson Imaging. 2018.
4. Kumar M, Nanga RPR, Verma G, Wilson N, Brisset JC, Nath K, et al. Emerging MR Imaging and Spectroscopic Methods to Study Brain Tumor Metabolism. Front Neurol. 2022;13:789355.
5. Nam KM, Gursan A, Bhogal AA, Wijnen JP, Klomp DWJ, Prompers JJ, et al. Deuterium echo-planar spectroscopic imaging (EPSI) in the human liver in vivo at 7 T. Magn Reson Med. 2023.
6. Yan H, Parsons DW, Jin G, McLendon R, Rasheed BA, Yuan W, Kos I, Batinic-Haberle I, Jones S, Riggins GJ, Friedman H, Friedman A, Reardon D, Herndon J, Kinzler KW, Velculescu VE, Vogelstein B, Bigner DD. IDH1 and IDH2 mutations in gliomas. N Engl J Med. 2009 Feb 19;360(8):765-73. doi: 10.1056/NEJMoa0808710. PMID: 19228619; PMCID: PMC2820383.
7. Christensen BC, Smith AA, Zheng S, Koestler DC, Houseman EA, Marsit CJ, Wiemels JL, Nelson HH, Karagas MR, Wrensch MR, Kelsey KT, Wiencke JK. DNA methylation, isocitrate dehydrogenase mutation, and survival in glioma. J Natl Cancer Inst. 2011 Jan 19;103(2):143-53. doi: 10.1093/jnci/djq497. Epub 2010 Dec 16. PMID: 21163902; PMCID: PMC3022619.
8. Liu Y, Lang F, Chou FJ, Zaghloul KA, Yang C. Isocitrate Dehydrogenase Mutations in Glioma: Genetics, Biochemistry, and Clinical Indications. Biomedicines. 2020 Aug 20;8(9):294. doi: 10.3390/biomedicines8090294. PMID: 32825279; PMCID: PMC7554955.
9. Horbinski C, Berger T, Packer RJ, Wen PY. Clinical implications of the 2021 edition of the WHO classification of central nervous system tumours. Nat Rev Neurol. 2022;18(9):515-29.
10. Alzial G, Renoult O, Paris F, Gratas C, Clavreul A, Pecqueur C. Wild-type isocitrate dehydrogenase under the spotlight in glioblastoma. Oncogene. 2022;41(5):613-21.
11. Horbinski C. What do we know about IDH1/2 mutations so far, and how do we use it? Acta Neuropathol. 2013 May;125(5):621-36. doi: 10.1007/s00401-013-1106-9. Epub 2013 Mar 20. PMID: 23512379; PMCID: PMC3633675.
12. Dang L, White DW, Gross S, Bennett BD, Bittinger MA, Driggers EM, Fantin VR, Jang HG, Jin S, Keenan MC, Marks KM, Prins RM, Ward PS, Yen KE, Liau LM, Rabinowitz JD, Cantley LC, Thompson CB, Vander Heiden MG, Su SM. Cancer-associated IDH1 mutations produce 2-hydroxyglutarate. Nature. 2009 Dec 10;462(7274):739-44. doi: 10.1038/nature08617. PMID: 19935646; PMCID: PMC2818760.
13. Atai NA, Renkema-Mills NA, Bosman J, Schmidt N, Rijkeboer D, Tigchelaar W, Bosch KS, Troost D, Jonker A, Bleeker FE, Miletic H, Bjerkvig R, De Witt Hamer PC, Van Noorden

CJ. Differential activity of NADPH-producing dehydrogenases renders rodents unsuitable models to study IDH1R132 mutation effects in human glioblastoma. J Histochem Cytochem. 2011 May;59(5):489-503. doi: 10.1369/0022155411400606. Epub 2011 Feb 10. PMID: 21527585; PMCID: PMC3201175.
14. Bisdas S, Chadzynski GL, Braun C, Schittenhelm J, Skardelly M, Hagberg GE, Ethofer T, Pohmann R, Shajan G, Engelmann J, Tabatabai G, Ziemann U, Ernemann U, Scheffler K. MR spectroscopy for in vivo assessment of the oncometabolite 2-hydroxyglutarate and its effects on cellular metabolism in human brain gliomas at 9.4T. J Magn Reson Imaging. 2016 Oct;44(4):823-33. doi: 10.1002/jmri.25221. Epub 2016 Mar 11. PMID: 26970248.
15. Chou FJ, Liu Y, Lang F, Yang C. D-2-Hydroxyglutarate in Glioma Biology. Cells. 2021;10(9).
16. Reiter-Brennan C, Semmler L, Klein A. The effects of 2-hydroxyglutarate on the tumorigenesis of gliomas. Contemp Oncol (Pozn). 2018;22(4):215-222. doi: 10.5114/wo.2018.82642. Epub 2018 Dec 31. PMID: 30783384; PMCID: PMC6377424.
17. Bi J, Chowdhry S, Wu S, Zhang W, Masui K, Mischel PS. Altered cellular metabolism in gliomas - an emerging landscape of actionable co-dependency targets. Nat Rev Cancer. 2020 Jan;20(1):57-70. doi: 10.1038/s41568-019-0226-5. Epub 2019 Dec 5. PMID: 31806884.
18. Masui K, Cavenee WK, Mischel PS. Cancer metabolism as a central driving force of glioma pathogenesis. Brain Tumor Pathol. 2016 Jul;33(3):161-8. doi: 10.1007/s10014-016-0265-5. Epub 2016 Jun 13. PMID: 27295313; PMCID: PMC5488809.
19. Masui K, Onizuka H, Cavenee WK, Mischel PS, Shibata N. Metabolic reprogramming in the pathogenesis of glioma: Update. Neuropathology. 2019 Feb;39(1):3-13. doi: 10.1111/neup.12535. Epub 2019 Jan 4. PMID: 30609184.
20. Zhang C, Moore LM, Li X, Yung WK, Zhang W. IDH1/2 mutations target a key hallmark of cancer by deregulating cellular metabolism in glioma. Neuro Oncol. 2013 Sep;15(9):1114-26. doi: 10.1093/neuonc/not087. Epub 2013 Jul 21. PMID: 23877318; PMCID: PMC3748922.
21. Birken DL, Oldendorf WH. N-acetyl-L-aspartic acid: a literature review of a compound prominent in 1H-NMR spectroscopic studies of brain. Neurosci Biobehav Rev. 1989 Spring;13(1):23-31. doi: 10.1016/s0149-7634(89)80048-x. PMID: 2671831.
22. Baslow, M.H. N -Acetylaspartate in the Vertebrate Brain: Metabolism and Function. N*eurochem Res* 28 , 941–953 (2003). https://doi.org/10.1023/A:1023250721185.
23. Namboodiri AM, Peethambaran A, Mathew R, Sambhu PA, Hershfield J, Moffett JR, Madhavarao CN. Canavan disease and the role of N-acetylaspartate in myelin synthesis. Mol Cell Endocrinol. 2006 Jun 27;252(1-2):216-23. doi: 10.1016/j.mce.2006.03.016. Epub 2006 May 2. PMID: 16647192.
24. Lieu, E.L., Nguyen, T., Rhyne, S. e*t al.* Amino acids in cancer. E*xp Mol Med* 52 , 15–30 (2020). https://doi.org/10.1038/s12276-020-0375-3.
25. Moffett JR, Ross B, Arun P, Madhavarao CN, Namboodiri AM. N-Acetylaspartate in the CNS: from neurodiagnostics to neurobiology. Prog Neurobiol. 2007 Feb;81(2):89-131. doi: 10.1016/j.pneurobio.2006.12.003. Epub 2007 Jan 5. PMID: 17275978; PMCID: PMC1919520.
26. Derbyshire E, Obeid R. Choline, Neurological Development and Brain Function: A Systematic Review Focusing on the First 1000 Days. Nutrients. 2020 Jun 10;12(6):1731. doi: 10.3390/nu12061731. PMID: 32531929; PMCID: PMC7352907.

27. McKnight TR SK, Chu PW, Chiu KS, Cloyd CP, Chang SM, Phillips JJ, Berger MS. Choline metabolism, proliferation, and angiogenesis in nonenhancing grades 2 and 3 astrocytoma. J Magn Reson Imaging. 2011 Apr, 21448944 -djP, PMC3076678 P.
28. Weinberg BD KM, Shim H, Mullins ME. Clinical Applications of Magnetic Resonance Spectroscopy in Brain Tumors: From Diagnosis to Treatment. Radiol Clin North Am. 2021 May, 33926682 -djrEMP, PMC8272438 P.
29. Jul DGBlmtdatcJCBFM, 22186669 -djEDP, PMC3390802 P.
30. Warburg O. On the origin of cancer cells. Science. 1956; 123 :309–314.
31. Cui XG, Han ZT, He SH, Wu XD, Chen TR, Shao CH, Chen DL, Su N, Chen YM, Wang T, Wang J, Song DW, Yan WJ, Yang XH, Liu T, Wei HF, Xiao J. HIF1/2α mediates hypoxia-induced LDHA expression in human pancreatic cancer cells. Oncotarget. 2017 Apr 11;8(15):24840-24852. doi: 10.18632/oncotarget.15266. PMID: 28193910; PMCID: PMC5421893.
32. Crawford FW KI, McGue C, et al. Relationship of pre-surgery metabolic and physiological MR imaging parameters to survival for patients with untreated GBM. J Neurooncol 2009, . -.
33. Tani, H.; Dulla, C.G.; Farzampour, Z.; Taylor-Weiner, A.; Huguenard, J.R.; Reimer, R.J. A local glutamate-glutamine cycle sustains synaptic excitatory transmitter release. Neuron 2014, 81, 888–900.
34. Boulland, J.L.; Rafiki, A.; Levy, L.M.; Storm-Mathisen, J.; Chaudhry, F.A. Highly dierential expression ofSN1, a bidirectional glutamine transporter, in astroglia and endothelium in the developing rat brain. Glia2003, 41, 260–275.
35. Featherstone DE. Intercellular glutamate signaling in the nervous system and beyond. ACS Chem Neurosci. 2010 Jan 20;1(1):4-12. doi: 10.1021/cn900006n. Epub 2009 Oct 9. PMID: 22778802; PMCID: PMC3368625.
36. Wise, D.R.; Deberardinis, R.J.; Mancuso, A.; Sayed, N.; Zhang, X.Y.; Pfeier, H.K.; Nissim, I.; Daikhin, E.;Yudko, M.; McMahon, S.B.; et al. Myc regulates a transcriptional program that stimulates mitochondrialglutaminolysis and leads to.
37. Ekici S, Nye JA, Neill SG, Allen JW, Shu HK, Fleischer CC. Glutamine Imaging: A New Avenue for Glioma Management. AJNR Am J Neuroradiol. 2022 Jan;43(1):11-18. doi: 10.3174/ajnr.A7333. Epub 2021 Nov 4. PMID: 34737183; PMCID: PMC8757564.
38. Trachtman H, Barbour R, Sturman JA, Finberg L. Taurine and osmoregulation: taurine is a cerebral osmoprotective molecule in chronic hypernatremic dehydration. Pediatr Res. 1988 Jan;23(1):35-9. doi: 10.1203/00006450-198801000-00008. PMID: 3340441.
39. Oja, S.S., Saransaari, P. Taurine as osmoregulator and neuromodulator in the brain. M*etab Brain Dis* 11 , 153–164 (1996). https://doi.org/10.1007/BF02069502.
40. Lallemand F, De Witte P. Taurine concentration in the brain and in the plasma following intraperitoneal injections. Amino Acids. 2004 Mar;26(2):111-6. doi: 10.1007/s00726-003-0058-0. Epub 2003 Dec 31. PMID: 15042438.
41. Roschel H, Gualano B, Ostojic SM, Rawson ES. Creatine Supplementation and Brain Health. Nutrients. 2021 Feb 10;13(2):586. doi: 10.3390/nu13020586. PMID: 33578876; PMCID: PMC7916590.
42. Kazak L, Cohen P. Creatine metabolism: energy homeostasis, immunity and cancer biology. Nat Rev Endocrinol. 2020 Aug;16(8):421-436. doi: 10.1038/s41574-020-0365-5. Epub 2020 Jun 3. PMID: 32493980.

43. Öz G, Deelchand DK, Wijnen JP, Mlynárik V, Xin L, Mekle R, Noeske R, Scheenen TWJ, Tkáč I; Experts' Working Group on Advanced Single Voxel 1H MRS. Advanced single voxel 1 H magnetic resonance spectroscopy techniques in humans: Experts' consensus recommendations. NMR Biomed. 2020 Jan 10:e4236. doi: 10.1002/nbm.4236. Epub ahead of print. PMID: 31922301; PMCID: PMC7347431.
44. Andronesi OC, Bhattacharyya PK, Bogner W, Choi IY, Hess AT, Lee P, Meintjes EM, Tisdall MD, Zaitzev M, van der Kouwe A. Motion correction methods for MRS: experts' consensus recommendations. NMR Biomed. 2021 May;34(5):e4364. doi: 10.1002/nbm.4364. Epub 2020 Jul 20. Erratum in: NMR Biomed. 2022 Jan;35(1):e4644. PMID: 33089547; PMCID: PMC7855523.
45. Považan M, Mikkelsen M, Berrington A, Bhattacharyya PK, Brix MK, Buur PF, Cecil KM, Chan KL, Chen DYT, Craven AR, Cuypers K, Dacko M, Duncan NW, Dydak U, Edmondson DA, Ende G, Ersland L, Forbes MA, Gao F, Greenhouse I, Harris AD, He N, Heba S, Hoggard N, Hsu TW, Jansen JFA, Kangarlu A, Lange T, Lebel RM, Li Y, Lin CE, Liou JK, Lirng JF, Liu F, Long JR, Ma R, Maes C, Moreno-Ortega M, Murray SO, Noah S, Noeske R, Noseworthy MD, Oeltzschner G, Porges EC, Prisciandaro JJ, Puts NAJ, Roberts TPL, Sack M, Sailasuta N, Saleh MG, Schallmo MP, Simard N, Stoffers D, Swinnen SP, Tegenthoff M, Truong P, Wang G, Wilkinson ID, Wittsack HJ, Woods AJ, Xu H, Yan F, Zhang C, Zipunnikov V, Zöllner HJ, Edden RAE, Barker PB. Comparison of Multivendor Single-Voxel MR Spectroscopy Data Acquired in Healthy Brain at 26 Sites. Radiology. 2020 Apr;295(1):171-180. doi: 10.1148/radiol.2020191037. Epub 2020 Feb 11. PMID: 32043950; PMCID: PMC7104702.
46. Kumar M, Nanga RPR, Verma G, Wilson N, Brisset JC, Nath K, Chawla S. Emerging MR Imaging and Spectroscopic Methods to Study Brain Tumor Metabolism. Front Neurol. 2022 Mar 16;13:789355. doi: 10.3389/fneur.2022.789355. PMID: 35370872; PMCID: PMC8967433.
47. Posse S, DeCarli C, Le Bihan D. Three-dimensional echo-planar MR spectroscopic imaging at short echo times in the human brain. Radiology. 1994 Sep;192(3):733-8. doi: 10.1148/radiology.192.3.8058941. PMID: 8058941.
48. Lin FH, Tsai SY, Otazo R, Caprihan A, Wald LL, Belliveau JW, Posse S. Sensitivity-encoded (SENSE) proton echo-planar spectroscopic imaging (PEPSI) in the human brain. Magn Reson Med. 2007 Feb;57(2):249-57. doi: 10.1002/mrm.21119. PMID: 17260356.
49. Prener M, Opheim G, Shams Z, Søndergaard CB, Lindberg U, Larsson HBW, Ziebell M, Larsen VA, Vestergaard MB, Paulson OB. Single-Voxel MR Spectroscopy of Gliomas with s-LASER at 7T. Diagnostics (Basel). 2023 May 19;13(10):1805. doi: 10.3390/diagnostics13101805. PMID: 37238288; PMCID: PMC10216996.
50. Liu ZL, Zhou Q, Zeng QS, Li CF, Zhang K. Noninvasive evaluation of cerebral glioma grade by using diffusion-weighted imaging-guided single-voxel proton magnetic resonance spectroscopy. J Int Med Res. 2012;40(1):76-84. doi: 10.1177/147323001204000108. PMID: 22429347.
51. Burger P.C., Dubois P.J., Schold S.C., Jr., Smith K.R., Jr., Odom G.L., Crafts D.C., Giangaspero F. Computerized tomographic and pathologic studies of the untreated, quiescent, and recurrent glioblastoma multiforme. J. *Neurosurg.* 1983; 58 :159–169. doi: 10.3171/jns.1983.58.2.0159.
52. Silbergeld DL, Chicoine MR. Isolation and characterization of human malignant glioma cells from histologically normal brain. J Neurosurg. 1997 Mar;86(3):525-31. doi: 10.3171/jns.1997.86.3.0525. PMID: 9046311.

53. Lemee J.M., Clavreul A., Menei P. Intratumoral heterogeneity in glioblastoma: Don't forget the peritumoral brain zone. N*euro-Oncology.* 2015; 17 :1322–1332.
54. Zetterling M, Roodakker KR, Berntsson SG, Edqvist PH, Latini F, Landtblom AM, Pontén F, Alafuzoff I, Larsson EM, Smits A. Extension of diffuse low-grade gliomas beyond radiological borders as shown by the coregistration of histopathological and magnetic resonance imaging data. J Neurosurg. 2016 Nov;125(5):1155-1166. doi: 10.3171/2015.10.JNS15583. Epub 2016 Feb 26. PMID: 26918468.
55. Pallud J, Varlet P, Devaux B, Geha S, Badoual M, Deroulers C, Page P, Dezamis E, Daumas-Duport C, Roux FX. Diffuse low-grade oligodendrogliomas extend beyond MRI-defined abnormalities. Neurology. 2010 May 25;74(21):1724-31. doi: 10.1212/WNL.0b013e3181e04264. PMID: 20498440.
56. Mortazavi A, Fayed I, Bachani M, Dowdy T, Jahanipour J, Khan A, Owotade J, Walbridge S, Inati SK, Steiner J, Wu J, Gilbert M, Yang CZ, Larion M, Maric D, Ksendzovsky A, Zaghloul KA. IDH-mutated gliomas promote epileptogenesis through d-2-hydroxyglutarate-dependent mTOR hyperactivation. Neuro Oncol. 2022 Sep 1;24(9):1423-1435. doi: 10.1093/neuonc/noac003. PMID: 34994387; PMCID: PMC9435503.
57. Andronesi OC, Loebel F, Bogner W, Marjańska M, Vander Heiden MG, Iafrate AJ, Dietrich J, Batchelor TT, Gerstner ER, Kaelin WG, Chi AS, Rosen BR, Cahill DP. Treatment Response Assessment in IDH-Mutant Glioma Patients by Noninvasive 3D Functional Spectroscopic Mapping of 2-Hydroxyglutarate. Clin Cancer Res. 2016 Apr 1;22(7):1632-41. doi: 10.1158/1078-0432.CCR-15-0656. Epub 2015 Nov 3. PMID: 26534967; PMCID: PMC4818725.
58. Guo J, Yao C, Chen H, Zhuang D, Tang W, Ren G, Wang Y, Wu J, Huang F, Zhou L. The relationship between Cho/NAA and glioma metabolism: implementation for margin delineation of cerebral gliomas. Acta Neurochir (Wien). 2012 Aug;154(8):1361-70; discussion 1370. doi: 10.1007/s00701-012-1418-x. Epub 2012 Jun 23. PMID: 22729482; PMCID: PMC3407558.
59. Yan G, Yi M, Li S, Yang L, Dai Z, Xuan Y, Wu R. Quantitative metabolic characteristics in the peritumoral region of gliomas at 7T. Technol Health Care. 2021;29(S1):509-517. doi: 10.3233/THC-218048. PMID: 33682787; PMCID: PMC8150443.
60. Klauser A, Klauser P, Grouiller F, Courvoisier S, Lazeyras F. Whole-brain high-resolution metabolite mapping with 3D compressed-sensing SENSE low-rank 1 H FID-MRSI. NMR Biomed. 2022 Jan;35(1):e4615. doi: 10.1002/nbm.4615. Epub 2021 Oct 1. PMID: 34595791; PMCID: PMC9285075.
61. Li X, Strasser B, Jafari-Khouzani K, Thapa B, Small J, Cahill DP, Dietrich J, Batchelor TT, Andronesi OC. Super-Resolution Whole-Brain 3D MR Spectroscopic Imaging for Mapping D-2-Hydroxyglutarate and Tumor Metabolism in Isocitrate Dehydrogenase 1-mutated Human Gliomas. Radiology. 2020 Mar;294(3):589-597. doi: 10.1148/radiol.2020191529. Epub 2020 Jan 7. PMID: 31909698; PMCID: PMC7053225.
62. An Z, Tiwari V, Baxter J, Levy M, Hatanpaa KJ, Pan E, Maher EA, Patel TR, Mickey BE, Choi C. 3D high-resolution imaging of 2-hydroxyglutarate in glioma patients using DRAG-EPSI at 3T in vivo. Magn Reson Med. 2019 Feb;81(2):795-802. doi: 10.1002/mrm.27482. Epub 2018 Sep 14. PMID: 30277274; PMCID: PMC6289635.
63. Czernicki T, Szeszkowski W, Marchel A, Gołebiowski M. Spectral changes in postoperative MRS in high-grade gliomas and their effect on patient prognosis. Folia Neuropathol. 2009;47(1):43-9. PMID: 19353433.

64. Andronesi OC, Loebel F, Bogner W, Marjańska M, Vander Heiden MG, Iafrate AJ, et al. Treatment Response Assessment in IDH-Mutant Glioma Patients by Noninvasive 3D Functional Spectroscopic Mapping of 2-Hydroxyglutarate. Clin Cancer Res. 2016;22(7):1632-41.
65. Lecocq A, Le Fur Y, Maudsley AA, Le Troter A, Sheriff S, Sabati M, Donnadieu M, Confort-Gouny S, Cozzone PJ, Guye M, Ranjeva JP. Whole-brain quantitative mapping of metabolites using short echo three-dimensional proton MRSI. J Magn Reson Imaging. 2015 Aug;42(2):280-9. doi: 10.1002/jmri.24809. Epub 2014 Nov 28. PMID: 25431032; PMCID: PMC4447620.
66. Donadieu M, Le Fur Y, Lecocq A, Maudsley AA, Gherib S, Soulier E, Confort-Gouny S, Pariollaud F, Ranjeva MP, Pelletier J, Guye M, Zaaraoui W, Audoin B, Ranjeva JP. Metabolic voxel-based analysis of the complete human brain using fast 3D-MRSI: Proof of concept in multiple sclerosis. J Magn Reson Imaging. 2016 Aug;44(2):411-9. doi: 10.1002/jmri.25139. Epub 2016 Jan 12. PMID: 26756662; PMCID: PMC4940345.
67. Reitman ZJ, Jin G, Karoly ED, Spasojevic I, Yang J, Kinzler KW, He Y, Bigner DD, Vogelstein B, Yan H. Profiling the effects of isocitrate dehydrogenase 1 and 2 mutations on the cellular metabolome. Proc Natl Acad Sci U S A. 2011 Feb 22;108(8):3270-5. doi: 10.1073/pnas.1019393108. Epub 2011 Feb 2. PMID: 21289278; PMCID: PMC3044380.
68. Sabatier J, Gilard V, Malet-Martino M, Ranjeva JP, Terral C, Breil S, Delisle MB, Manelfe C, Tremoulet M, Berry I. Characterization of choline compounds with in vitro 1H magnetic resonance spectroscopy for the discrimination of primary brain tumors. Invest Radiol. 1999 Mar;34(3):230-5. doi: 10.1097/00004424-199903000-00013. PMID: 10084669.
69. Jalbert LE, Elkhaled A, Phillips JJ, Neill E, Williams A, Crane JC, Olson MP, Molinaro AM, Berger MS, Kurhanewicz J, Ronen SM, Chang SM, Nelson SJ. Metabolic Profiling of IDH Mutation and Malignant Progression in Infiltrating Glioma. Sci Rep. 2017 Mar 22;7:44792. doi: 10.1038/srep44792. PMID: 28327577; PMCID: PMC5361089.
70. Pope WB, Prins RM, Albert Thomas M, Nagarajan R, Yen KE, Bittinger MA, Salamon N, Chou AP, Yong WH, Soto H, Wilson N, Driggers E, Jang HG, Su SM, Schenkein DP, Lai A, Cloughesy TF, Kornblum HI, Wu H, Fantin VR, Liau LM. Non-invasive detection of 2-hydroxyglutarate and other metabolites in IDH1 mutant glioma patients using magnetic resonance spectroscopy. J Neurooncol. 2012 Mar;107(1):197-205. doi: 10.1007/s11060-011-0737-8. Epub 2011 Oct 21. PMID: 22015945; PMCID: PMC3650613.
71. Bulik M, Kazda T, Slampa P, Jancalek R. The Diagnostic Ability of Follow-Up Imaging Biomarkers after Treatment of Glioblastoma in the Temozolomide Era: Implications from Proton MR Spectroscopy and Apparent Diffusion Coefficient Mapping. Biomed Res Int. 2015;2015:641023. doi: 10.1155/2015/641023. Epub 2015 Sep 13. PMID: 26448943; PMCID: PMC4584055.
72. Cui Y, Zeng W, Jiang H, Ren X, Lin S, Fan Y, Liu Y, Zhao J. Higher Cho/NAA Ratio in Postoperative Peritumoral Edema Zone Is Associated With Earlier Recurrence of Glioblastoma. Front Neurol. 2020 Dec 4;11:592155. doi: 10.3389/fneur.2020.592155. PMID: 33343496; PMCID: PMC7747764.
73. Hamberger, A.; Nyström, B.; Larsson, S.; Silfvenius, H.; Nordborg, C. Amino acids in the neuronalmicroenvironment of focal human epileptic lesions. Epilepsy Res. 1991, 9, 32–43.
74. Natarajan SK, Venneti S. Glutamine Metabolism in Brain Tumors. Cancers (Basel). 2019 Oct 24;11(11):1628. doi: 10.3390/cancers11111628. PMID: 31652923; PMCID: PMC6893651.
75. Leung, E., Cairns, R.A., Chaudary, N. e*t al.* Metabolic targeting of HIF-dependent glycolysis reduces lactate, increases oxygen consumption and enhances response to high-dose

single-fraction radiotherapy in hypoxic solid tumors. B*MC Cancer* 17 , 418 (2017). https://doi.org/10.1186/s12885-017-3402-6.
76. Koivunen, P., Lee, S., Duncan, C. e*t al.* Transformation by the (R)-enantiomer of 2-hydroxyglutarate linked to EGLN activation. N*ature* 483 , 484–488 (2012). https://doi.org/10.1038/nature10898.
77. Chesnelong C, Chaumeil MM, Blough MD, Al-Najjar M, Stechishin OD, Chan JA, Pieper RO, Ronen SM, Weiss S, Luchman HA, Cairncross JG. Lactate dehydrogenase A silencing in IDH mutant gliomas. Neuro Oncol. 2014 May;16(5):686-95. doi: 10.1093/neuonc/not243. Epub 2013 Dec 22. PMID: 24366912; PMCID: PMC3984548.
78. Goryawala M, Saraf-Lavi E, Nagornaya N, Heros D, Komotar R, Maudsley AA. The Association between Whole-Brain MR Spectroscopy and IDH Mutation Status in Gliomas. J Neuroimaging. 2020 Jan;30(1):58-64. doi: 10.1111/jon.12685. Epub 2019 Dec 23. PMID: 31868291; PMCID: PMC7485119.
79. Kallenberg K, Bock HC, Helms G, Jung K, Wrede A, Buhk JH, Giese A, Frahm J, Strik H, Dechent P, Knauth M. Untreated glioblastoma multiforme: increased myo-inositol and glutamine levels in the contralateral cerebral hemisphere at proton MR spectroscopy. Radiology. 2009 Dec;253(3):805-12. doi: 10.1148/radiol.2533071654. Epub 2009 Sep 29. PMID: 19789222.